UNIVERSITY OF CALGARY

UAV-LiDAR and Structure from Motion Photogrammetry: Spatial Accuracy in Vegetated Terrain

by

Maja Kucharczyk

A THESIS

SUBMITTED TO THE FACULTY OF GRADUATE STUDIES

IN PARTIAL FULFILMENT OF THE REQUIREMENTS FOR THE

DEGREE OF MASTER OF SCIENCE

GRADUATE PROGRAM IN GEOGRAPHY

CALGARY, ALBERTA

JULY, 2017

© Maja Kucharczyk 2017

Abstract

Multiview stereo images acquired by uninhabited / unmanned aerial vehicles (UAVs) in combination with structure from motion (SfM) photogrammetry have created new capacity to develop high-resolution geospatial data, but vertical error is typically higher in vegetated areas because the ground surface is not visible in stereo. Miniaturized LiDAR systems for UAVs have potential to overcome this limitation, but their vertical accuracy in different vegetation types is not well documented. This thesis evaluated the accuracy of UAV-LiDAR and UAV-SfM in six vegetation types: grasses (short and tall), shrubs (short and tall), and trees (deciduous and coniferous). Results indicate UAV-LiDAR was more accurate in estimating ground elevation in all types, while vegetation height accuracy was higher for some types with UAV-SfM. UAV-LiDAR consistently sampled sub-canopy tree structure, while UAV-SfM only captured tree tops. Several factors are proposed to explain these differences and direct future research.

Acknowledgements

I would like to thank my supervisor Dr. Chris Hugenholtz for your mentorship, generosity, encouragement, and overall infectious enthusiasm. Thank you for giving me numerous opportunities that have contributed to my development as a research student. Thank you to my proposal committee, Dr. Mryka Hall-Beyer and Dr. Geoffrey Hay, for helping to shape my research with your suggestions and important questions. Thank you to my examination committee, Dr. Mryka Hall-Beyer and Dr. Derek Lichti, for your time in reviewing this thesis and providing feedback. Thank you to my fellow lab mates for your review of my presentations and writing over the past two years – the comradery of our lab has given me extra support throughout my program. Thanks to Xueyang Zou and Paul Nesbit, with whom I've shared many brainstorming sessions and long days in the field. Thank you endlessly to my dear mom, dad, brother, and beagle for your continued unconditional support as I pursue my studies far away from you. Your love and encouragement mean everything to me.

Table of contents

List of tables

List of figures

List of abbreviations and symbols

<	less than
>	greater than
≤	less than or equal to
°	degree
3D	three dimensional
AGL	above ground level
ASPRS	American Society for Photogrammetry and Remote Sensing
BCAL	Boise Center Aerospace Laboratory
CGVD28	Canadian Geodetic Vertical Datum of 1928
cm	centimeter
cm^3	cubic centimeter
CSF	Cloth Simulation Filter
CSRS	Canadian Spatial Reference System
DCHM	digital canopy height model
DEM	digital elevation model
DSM	digital surface model
DTM	digital terrain model
GCP	ground control point
GNSS	Global Navigation Satellite System
h_{DCHM}	DCHM-derived vegetation height measurement
h_{LiDAR}	LiDAR-derived vegetation height measurement
h_{ref}	reference vegetation height measurement
IDW	inverse distance weighted
IMU	inertial measurement unit
kg	kilogram
km	kilometer
km^2	square kilometer
LiDAR	light detection and ranging
m	meter

m^2	square meter
MCC	Multiscale Curvature Classification
min	minute
mm	millimeter
MP	megapixel
MVS	multiview stereo
n	number of samples
NAD83	North American Datum of 1983
nm	nanometer
NVA	non-vegetated vertical accuracy
PPP	precise point positioning
pts/m^2	points per square meter
Q_{95}	95^{th} percentile absolute error
RGB	red green blue
RMSE	root mean square error
$RMSE_r$	horizontal linear RMSE in the radial direction
$RMSE_x$	RMSE in the x-direction
$RMSE_y$	RMSE in the y-direction
RTK	real-time kinematic
s	second
SfM	structure from motion
t	curvature tolerance parameter
TIN	triangulated irregular network
UAV	uninhabited / unmanned aerial vehicle
UAV-LiDAR	UAV-based LiDAR
UAV-SfM	UAV-based SfM-MVS
USD	United States dollar
UTM	Universal Transverse Mercator
VVA	vegetated vertical accuracy
z_{DTM}	DTM-derived ground elevation measurement
z_{LiDAR}	LiDAR point-derived ground elevation measurement

z_{ref}	reference ground elevation measurement
α	alpha
λ	scale parameter

Chapter 1: Introduction

1.1 Background

The application of remote sensing technology to 'see' through vegetation canopy in order to resolve the underlying structure and terrain is important for research and commercial applications involving geoscience, forestry, ecology, and engineering (Bater & Coops, 2009). Whether vegetation is the focus of a study or the feature being removed in order to uncover terrain features, a goal ubiquitous to 3D mapping of vegetation is to accurately reconstruct the ground surface (Bater & Coops, 2009). Accurate topography is vital not only for surficial studies, but is essential for related measurements of vegetation structure and biomass (St-Onge et al., 2008; Vastaranta et al., 2013). Prior to the widespread adoption of active remote sensing techniques, options for 3D mapping in vegetated terrain were limited – ground-based surveys were time-consuming, and stereo-pair photogrammetry had to be supplemented by field topographic surveys under dense vegetation (Véga & St-Onge, 2008; Tang & Shao, 2015). The advent of light detection and ranging (LiDAR) resolved these issues.

1.1.1 Light detection and ranging (LiDAR)

LiDAR is an active form of remote sensing, whereby the LiDAR sensor emits a laser pulse, which is then reflected off the target object and returned to the sensor. The LiDAR system converts each return into a 3D point. The 3D coordinates of a LiDAR point are computed using many factors. First, given the speed of light and the precise time it took the laser pulse to travel back to the sensor, the range (distance) from the sensor to the target object can be calculated. With the range, the scan angle of the laser pulse, the horizontal and vertical position of the sensor, and the angular orientation of the sensor, the 3D coordinates of the point can be calculated (Slattery & Slattery, 2013).

By recording thousands of measurements per second, LiDAR point clouds can contain millions of points (or more), resulting in a rich 3D dataset. When the LiDAR laser pulse diameter is not fully reflected by one object, the remainder of the laser pulse travels past the first object and reflects off a second object. This is called the second return. Multiple-return LiDAR sensors emit laser pulses that return two or more times. The multiple-return nature of LiDAR sensors is especially useful for obtaining 3D point measurements of vegetated areas. The LiDAR sensor

receives laser pulse returns from vegetation, as well as from the underlying ground surface (Lisein et al., 2013). Terrestrial (ground-based) LiDAR has been used for topographic mapping, but its efficiency can be hindered when highly oblique acquisition angles experience occlusions and multiple scanning locations are required. Airborne LiDAR, on the other hand, has revolutionized the collection of large point clouds over large areas, giving rise to a new era of 3D mapping.

1.1.2 Airborne LiDAR for vegetation monitoring

The integration of LiDAR sensors with piloted aircraft has provided high areal coverage and spatial resolution, and capabilities to 'see' through vegetation to the underlying terrain, which are essential for a wide array of mapping applications (Bater & Coops, 2009). For example, forest management requires detailed, sometimes tree-level, information including stem counts, tree heights, crown base heights, diameter at breast heights, and biomass (Kwak et al., 2007). Small-footprint LiDAR has been shown to provide such biophysical parameters (Jensen & Mathews, 2016). Additionally, the time and cost estimates of traditional field methods versus airborne LiDAR for surveying 200 acres (0.81 km^2) of forest have been estimated to be 14 weeks and $32,000 versus 4 weeks and $16,000, respectively (Means & Acker, 2000).

Airborne LiDAR has been shown to reduce time and cost relative to traditional field surveys of moderately large areas. However, for applications such as the regular monitoring of biomass over very large areas (> 100 km^2), repeatedly chartering piloted aircraft for LiDAR collection is financially unfeasible (St-Onge et al., 2008). For example, Erdody and Moskal (2010) showed that the cost of acquiring airborne LiDAR data over a 500 km^2 study area at a suitable point density (i.e., 6-8 points/m^2) was $150,000 USD plus $10,000-20,000 USD for mobilization costs. As a solution to the high cost of airborne LiDAR data, archived LiDAR terrain measurements have been combined with repeat satellite stereo-pair photogrammetry of the canopy surface (St-Onge et al., 2008). Conversely, for small-area (< 10 km^2) mapping, it may not be feasible to charter piloted aircraft even once. For this reason, high density 3D mapping with uninhabited / unmanned aerial vehicles (UAVs) has gained popularity as a flexible and cost-effective alternative.

1.1.3 Uninhabited / unmanned aerial vehicles (UAVs)

Within the past decade, the use of small UAVs for topographic mapping in the geosciences has increased dramatically. This surge is due to technological advances across multiple disciplines, including miniaturization of navigational sensors (i.e., Global Navigation Satellite System [GNSS] receivers, inertial measurement units [IMUs]), and autopilot computers to fit onboard small (< 25 kg) fixed wing and multi-rotor platforms. With an autopilot, a flight plan consisting of waypoints can be pre-programmed and uploaded to the UAV for semi-autonomous flight, with user intervention possible through radio-link telemetry and flight control software at the ground station.

1.1.4 UAV-based structure from motion-multiview stereo (SfM-MVS)

Equally important to the advancement of flight hardware and software was the emergence of structure from motion-multiview stereo (SfM-MVS) photogrammetry – a derivative of traditional photogrammetry with less stringent hardware requirements for both the platform and imaging system. SfM-MVS generally consists of the following steps. First, computer vision algorithms search through each image to identify 'features' – that is, individual pixels that are robust to changes in scale, illumination, and 3D viewing angle (Carrivick et al., 2016). Next, the features are assigned unique 'descriptors', which allow for the same features to be identified across multiple images and for the images to be approximately aligned. This initial image alignment is iteratively optimized via bundle adjustment algorithms, the output of which is a sparse 3D point cloud of feature correspondences (Westoby et al., 2012). Multiview stereo (MVS) algorithms then densify the sparse point cloud, typically by two or more orders of magnitude (Westoby et al., 2012). For scaling and orientation, the point cloud may be assigned relative or absolute (i.e., real-world) coordinates through the input of ground control points (GCPs). The densified point cloud is commonly used to make raster products, namely orthomosaics and digital elevation models (DEMs).

This ability to reconstruct landform geometry from MVS imagery acquired with off-the-shelf digital cameras was made possible by advances in computer vision algorithms, and – along with user-friendly commercial SfM-MVS software – has allowed UAV-based remote sensing to flourish as an inexpensive and accessible alternative to airborne LiDAR. Geoscience case studies have used UAV-based SfM-MVS (hereafter UAV-SfM) to develop high-resolution 3D maps of:

aeolian landforms (Hugenholtz et al., 2013), ultrafine fault zones (Johnson et al., 2014), fluvial environments (Tamminga et al., 2015), aggregate stockpiles (Hugenholtz et al., 2015), glaciers (Whitehead et al., 2013), landslides (Niethammer et al., 2012), and more. UAV-SfM raster products in non-vegetated terrain have been shown to be accurate within 3 cm (Hugenholtz et al., 2016), rivaling airborne LiDAR spatial accuracy. The vulnerabilities of UAV-SfM, however, are exposed in vegetated terrain, where the following challenges may arise: (i) dense vegetation may cause substantial occlusion of the ground surface, resulting in low feature matching across images and poor reconstruction of the ground surface, (ii) wind-blown vegetation, like any non-static feature, can create difficulties in feature matching, and (iii) vegetation's complex structure may be difficult to reconstruct (Lisein et al., 2013; Carrivick et al., 2016). Previous studies using UAV-SfM to reconstruct topography have consistently reported decreased accuracy in areas of vegetation (Dandois & Ellis, 2010, 2013; Hugenholtz et al., 2013, 2016; Jensen & Mathews, 2016).

1.1.5 UAV-based LiDAR

To address the financial and logistical challenges of piloted airborne LiDAR, as well as issues UAV-SfM experiences acquiring data below the vegetation canopy, one emerging solution is to use a miniaturized LiDAR and allied components on a UAV. UAV-LiDAR systems can fly at lower altitudes and speeds than piloted aircraft, resulting in a higher point density than traditional piloted airborne LiDAR surveys. Higher point density could improve the accuracy of vegetation height measurements by: (i) increasing the likelihood laser pulses penetrate through the forest canopy and measure the ground surface, and (ii) increasing the likelihood of sampling tree tops (Hodgson & Bresnahan, 2004; Wallace et al., 2014). Additionally, the smaller footprint diameters associated with lower flying altitudes increase the likelihood the laser pulse is able to penetrate the forest canopy and reach the ground surface (Hodgson & Bresnahan, 2004).

1.2 Research motivation, objectives, and thesis overview

Research has shown that piloted LiDAR accuracy varies with vegetation type (Gaveau & Hill, 2003; Clark et al., 2004; Hodgson & Bresnahan, 2004; Hodgson et al., 2005; Hopkinson et al., 2005; Andersen et al., 2006). The consensus is that laser pulse penetration varies with changes of vegetation structure and density across trees, grasses, and shrubs (Gaveau & Hill, 2003).

However, little evidence has been presented to date regarding the spatial accuracy of UAV-LiDAR systems in vegetated terrain, and no known testing has been done in settings where the vegetation type varies considerably.

As with UAV-LiDAR, previous studies assessing the spatial accuracy of UAV-SfM in vegetated terrain have done so with a limited diversity of vegetation types. Similar to UAV-LiDAR, UAV-SfM may also experience variable occlusion of the ground surface with changing vegetation structure and density. The very high spatial resolution imagery (typically 5 cm or finer) afforded by UAV-SfM may be able to capture the exposed ground surface more adequately in some vegetation types than others.

Considering the lack of evidence demonstrating UAV-LiDAR and UAV-SfM performance in different types of vegetation, *the objective of this research was to evaluate the accuracy of these techniques for estimating the ground surface elevation and vegetation height at a study site consisting of six major vegetation types: coniferous trees, deciduous trees, short grass, tall grass, short shrubs, and tall shrubs.* The thesis is structured in two parts to address this objective. Chapter 2 assesses the spatial accuracy of the UAV-LiDAR data. Horizontal, vertical (ground surface elevation), and vegetation height accuracies were calculated using field-based reference measurements. Vertical accuracy was calculated at LiDAR point locations in order to eliminate error due to interpolation. Vertical and vegetation height accuracies were calculated per vegetation type, and statistical tests were performed to determine if errors between vegetation types were significant. Horizontal and vertical accuracies at the 95% confidence level were evaluated according to the 2015 American Society for Photogrammetry and Remote Sensing (ASPRS) Positional Accuracy Standards for Digital Geospatial Data (ASPRS, 2015). The horizontal, vertical, and vegetation height errors of the UAV-LiDAR system were compared with previously reported errors of data acquired from piloted LiDAR, UAV-LiDAR, and UAV-SfM in vegetated terrain.

Chapter 3 assesses the vertical and vegetation height accuracies of UAV-SfM data acquired at the same study site. Similar to Chapter 2, vertical and vegetation height accuracies were calculated for each vegetation type, and statistical tests were performed to determine if errors between vegetation types were significant. The vertical accuracy of the UAV-SfM dataset was assessed at the 95% confidence level (ASPRS, 2015). Additionally, the UAV-SfM vertical and vegetation height errors were compared to the UAV-LiDAR errors from Chapter 2. Factors

contributing to the differences in vertical and vegetation height errors between the datasets were examined and discussed.

Chapter 4 summarizes the major findings and research contributions of Chapters 2 and 3, and examines the limitations of the research. Finally, perspectives are offered on future work.

It is important to note that because Chapters 2 and 3 have been prepared as separate manuscripts for publication, there is some overlap in the descriptions of the study site and methodology.

Chapter 2: UAV-LiDAR accuracy assessment in vegetated terrain

2.1 Chapter abstract

This chapter examines the accuracy of ground surface elevation and vegetation height derived from UAV-LiDAR data at a field site with six different vegetation types: coniferous trees, deciduous trees, short grass, tall grass, short shrubs, and tall shrubs. The LiDAR data were acquired from a single-rotor vertical takeoff and landing UAV equipped with Riegl VUX-1UAV laser scanner, KVH Industries 1750 inertial measurement unit, and dual NovAtel GNSS receivers. Field reference measurements of ground surface elevation and vegetation height were acquired with conventional field surveying methods. Accuracy was evaluated using methods outlined in the 2015 American Society for Photogrammetry and Remote Sensing (ASPRS) Positional Accuracy Standards for Digital Geospatial Data. Results show that the horizontal accuracy and vegetated vertical accuracy (VVA) at the 95% confidence level were 0.05 m and 0.24 m, respectively. Vertical errors (95^{th} percentile absolute) ranged from 0.06 m under coniferous trees to 0.11 m under deciduous trees, with median errors significantly above 0.00 m for all classes except short grass and coniferous trees. According to the 2015 ASPRS standards, the reported errors fulfill the requirements for horizontal and vertical mapping at the 6 cm and 8 cm RMSE levels, respectively. Vegetation height errors (95^{th} percentile absolute) ranged from 0.28 m in short grass to 3.31 m in coniferous trees. These errors were higher than expected, but may be a result of low point density. In terms of 95^{th} percentile absolute errors, vertical (ground surface elevation errors) differed only by 0.05 m between the vegetation types, while vegetation height errors different by 3.03 m, highlighting the importance of considering vegetation type-specific errors for vegetation height mapping applications.

2.2 Introduction

The proliferation of light detection and ranging (LiDAR) in remote sensing has revolutionized 3D mapping. Since the 1990s, the large-area surveying capabilities of piloted airborne LiDAR have been applied to city-wide engineering surveys, forest mensuration, geo-hazards, and various topographic mapping studies (Madden et al., 2015). The ability of LiDAR to penetrate layers of vegetation and measure the underlying topography provides an unprecedented ability to ‘separate’ the vegetation and ground surface with high detail and accuracy. This capability has

allowed LiDAR to become a reference standard for mapping vegetated structure and underlying terrain, virtually eliminating traditional photogrammetry from use in applications like forestry (Tang & Shao, 2015).

For small-area mapping applications (i.e., less than a few km^2), the financial and logistical challenges of chartering piloted aircraft equipped with LiDAR sensors can hinder timely and cost-effective data collection. Uninhabited / unmanned aerial vehicles (UAVs) have emerged as a viable, cost-effective alternative for many small- (< 1 km^2) to moderate-area (1 – 10 km^2) mapping campaigns, but the bulk of research and commercial applications to date have focused on optical imagery acquired by UAVs, often involving consumer-grade RGB cameras. Research has shown that multiview stereo (MVS) imagery acquired from UAVs combined with structure from motion (SfM) photogrammetric image processing yields high accuracy, survey-grade 3D data (Whitehead & Hugenholtz, 2014; Hugenholtz et al., 2015, 2016). The caveat, however, is vegetated terrain, where detection of the ground surface and other features is limited by occlusion, leading to poor reconstruction of the vegetation structure and underlying topography during SfM processing (Dandois & Ellis, 2010, 2013; Lisein et al., 2013; Hugenholtz et al., 2013, 2016; Jensen & Mathews, 2016; Wallace et al., 2016).

UAV-based LiDAR has been proposed as a solution to the limitations of UAV-based SfM-MVS (hereafter UAV-SfM). Rather than eliminating occlusions completely, the notion is that a LiDAR system on a UAV should be able to penetrate vegetation, reduce occlusions, and improve detection of the ground surface and sub-canopy vegetation structure. Several studies have quantified UAV-LiDAR accuracy in vegetated settings (Wallace et al., 2012, 2014, 2016). Wallace et al. (2012) assessed the horizontal and vertical accuracy of UAV-LiDAR data in vegetated terrain using 130 high reflectivity artificial targets. The horizontal and vertical root mean square errors (RMSE) were 0.60 m and 0.19 m, respectively. Wallace et al. (2014) assessed the vegetation height accuracy of the same UAV-LiDAR system from 248 single-species trees distributed among six plots with mean tree heights ranging from 5.71 to 8.93 m – the vegetation height RMSE was 0.52 m. Wallace et al. (2016) assessed the horizontal and vertical accuracy of the same system using 10 artificial targets, and vegetation height accuracy using 122 single-species trees with heights ranging from 4.7 m to 16.2 m. Their horizontal, vertical, and vegetation height RMSEs were 0.42 m, 0.17 m, and 0.92 m, respectively.

The use of high reflectivity artificial targets to assess vertical accuracy does not test the system's ability to penetrate vegetation to measure the underlying ground elevation. Measuring the vertical error of LiDAR points reflected off vegetated terrain would provide more realistic information for operational situations. Additionally, as vegetation structure varies across canopy, herbaceous, and shrubby plant layers, so does the laser pulse's ability to penetrate those layers (Gaveau & Hill, 2003). Therefore, it is important to test vertical accuracy in various vegetation types, as was done for piloted LiDAR data by Hodgson and Bresnahan (2004). In the same regard, it is important to evaluate vegetation height accuracy using various vegetation types in order to discriminate how different structures affect the LiDAR signal and resulting measurements. A final missing element from previous UAV-LiDAR studies is to place the accuracies into context with the 2015 American Society for Photogrammetry and Remote Sensing (ASPRS) accuracy reporting standards for geospatial data (ASPRS, 2015). This provides a benchmark for research and professional applications.

Given the potential of UAV-LiDAR and growing demand for commercial UAV mapping products, we performed a case study to assess spatial accuracy at a site with six major vegetation functional groups: coniferous trees, deciduous trees, short grass, tall grass, short shrubs, and tall shrubs. For checkpoint quantity, spatial distribution, accuracy calculation, reporting, and more, we followed the 2015 ASPRS standards. Our assessment quantified the horizontal and vertical accuracies, as well as the vegetation height accuracy. Based on previous accuracy assessments of LiDAR data acquired from piloted aircraft (e.g., Gaveau & Hill, 2003; Clark et al., 2004; Hodgson & Bresnahan, 2004; Hodgson et al., 2005; Hopkinson et al., 2005; Andersen et al., 2006), we hypothesized that the UAV-LiDAR vertical accuracy would vary with vegetation type.

2.3 Study site

The study site is located near Bragg Creek, Alberta, Canada (50°53'24"N, 114°42'26"W), and occupies approximately 250 x 400 m of very gently sloping terrain (3° mean slope) (Figure 2.1). The perimeter and area of the site are 1.25 km and 0.10 km^2, respectively. Vegetation types present consist of coniferous trees, deciduous trees, short grass (0-0.3 m height), tall grass (> 0.3 m height), short shrubs (0-1 m height), and tall shrubs (> 1 m height) (Figure 2.2). The coniferous trees are dominated by Lodgepole Pine (*Pinus contorta*) with occasional White Spruce (*Picea glauca*). The deciduous trees are dominated by Balsam Poplar (*Populus*

balsamifera). Shrubs consist of Shrubby Cinquefoil (*Dasiphora fruticose*), Bog Birch (*Betula pumila*), and Sandbar Willow (*Salix exigua*). The site also contains a pipeline right of way and a reclaimed natural gas well pad. The natural gas well pad is a fenced area that contains tall grasses whose minimum heights defined the minimum height of the tall grass class and the maximum height of the short grass class. Additional tall grass patches are located outside of the fenced natural gas well pad, distributed among the short grass areas. The site is occasionally grazed by livestock, which likely explains why the grass within the fenced area is tall (i.e., protection from grazers), while the grass outside the fenced area is predominantly short and grazed. The short and tall shrub class height ranges were defined based on strong spatial clustering of the two classes – short shrubs dominated the southern half of the site and had 0-1 m heights, while the shrubs that dominated the northern half were taller than 1 m.

Figure 2.1 Study site location and general distribution of the six vegetation types (coniferous trees, deciduous trees, short grass, tall grass, short shrubs, and tall shrubs).

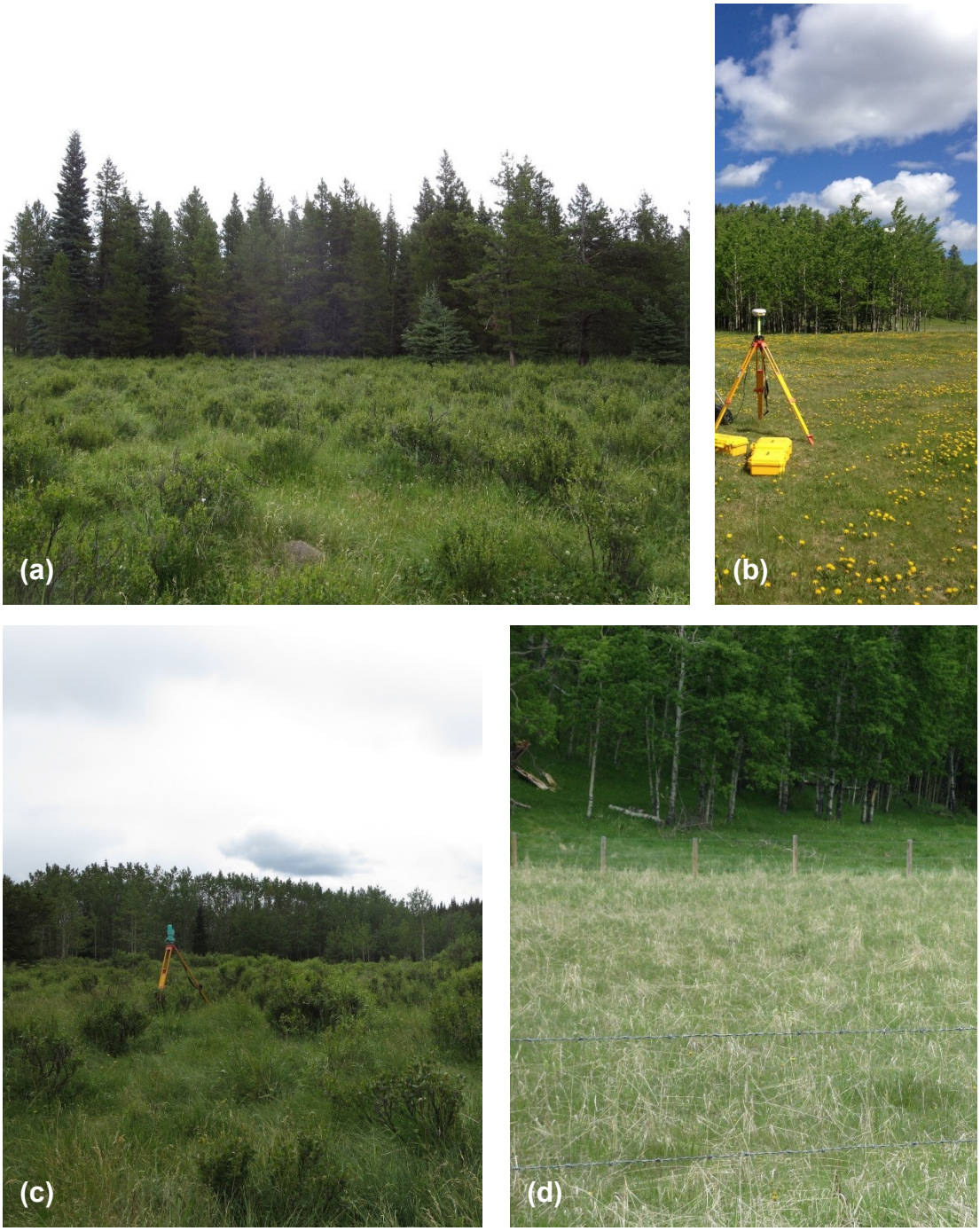

Figure 2.2 Examples of the vegetation types present throughout the study site: (a) short shrubs (foreground) and coniferous trees (background), (b) short grass (foreground) and deciduous trees (background), (c) tall shrubs (foreground) and deciduous trees (background), and (d) tall grass.

2.4 Methods

2.4.1 UAV-LiDAR system

The UAV consisted of a custom-designed, gas-powered rotary wing platform equipped with a Riegl VUX-1UAV-LiDAR sensor (Figure 2.3). The UAV has a maximum take-off weight of 35 kg, rotor diameter of 2 m, airframe length of 2.5 m, and flight time of 1-2 hours depending on payload, site altitude, and wind. The main components include an 80 cm^3 gas engine, dual-antenna NovAtel GNSS for sensor position and heading, and a modular payload configuration capable of holding up to three different sensors simultaneously. The Riegl VUX-1UAV is integrated with a tactical-grade KVH 1750 IMU. Additional LiDAR sensor specifications are summarized in Table 2.1.

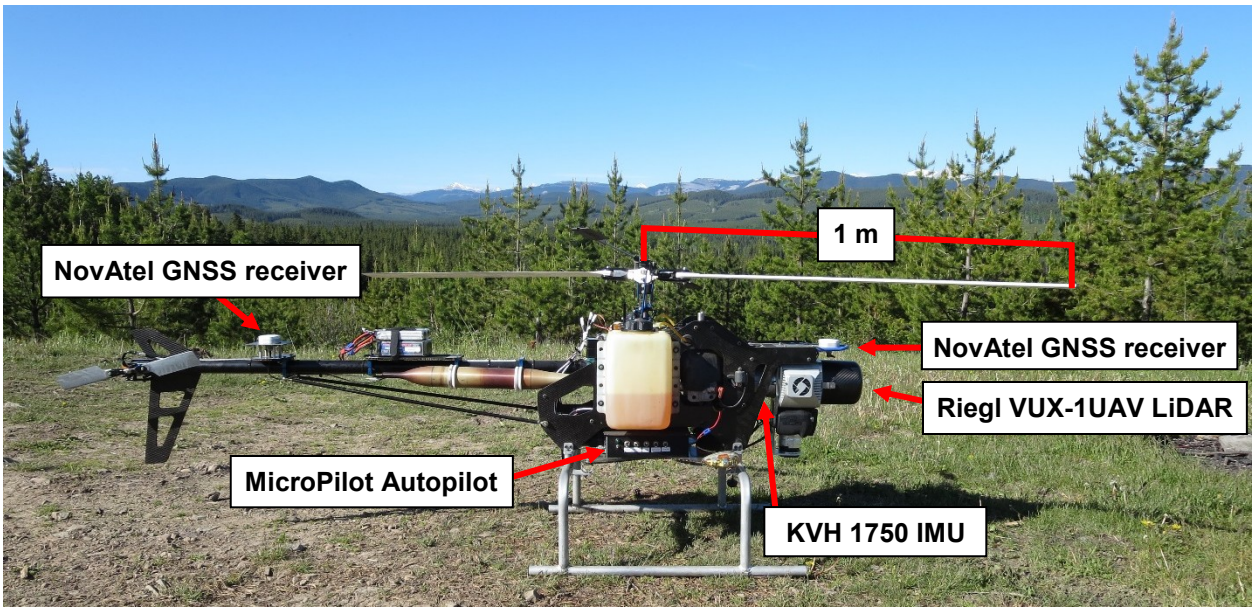

Figure 2.3 UAV-LiDAR platform and components.

Table 2.1 UAV-LiDAR system attributes.

System attribute	Properties
Rotor diameter	2 m
Maximum take-off weight	35 kg
Power source	80 cm^3 gas engine
Maximum flight time	1-2 hours
LiDAR sensor	Riegl VUX1-UAV
Laser wavelength	1550 nm
Scan pattern	Unidirectional and parallel
Maximum scan speed	200 scans/s
Maximum effective measurement rate	500,000 points/s
Maximum number of returns	5
Maximum operating flight altitude	350 m
Field of view	330°
Dimensions	227 x 180 x 125 mm
Weight	3.5 kg

2.4.2 LiDAR data acquisition

The UAV flight was conducted during leaf-on conditions prior to the peak of the growing season, providing near-maximum leaf cover. During the flight, the LiDAR system acquired measurements from 60 m above ground level (AGL). Additional flight and data acquisition parameters are summarized in Table 2.2.

Table 2.2 UAV-LiDAR flight and data acquisition parameters.

Flight parameter	Properties
Flight date	02 June 2016
Flight altitude	60 m AGL
Aircraft speed	15 knots (7.7 m/s)
Number of flight lines and orientation	4 (parallel)
Point observations acquired	5,399,697
Average point density	57 pts/m^2
Average point spacing	0.13 m
Ground-classified points (% of total)	1,086,968 (20%)
Average ground point density	11 pts/m^2
Average ground point spacing	0.30 m
Horizontal coordinate system and datum	UTM Zone 11N NAD 83
Vertical datum	CGVD28

2.4.3 LiDAR data processing

Initial processing of the raw LiDAR data included integration of data from the GNSS, IMU, raw scans, and ground control points (GCPs). Terrasolid TerraScan software was used for point cloud classification to separate 'ground' from 'non-ground' points. The software uses a point classification algorithm by Axelsson (1999) (Maltamo et al., 2004; Gatziolis et al., 2010, Zhang et al., 2016). This algorithm works by first applying a grid to the points (user-specified cell size) and classifying the lowest point within each cell as ground. These ground points are used to construct an initial triangulated irregular network (TIN). Then, additional points are classified as ground and are added to the TIN if they are within user-specified distance and angle thresholds. The program iterates the TIN densification until no additional points can be classified as ground (Axelsson, 1999).

2.4.3.1 Ground elevation extraction

Following point classification, 100 ground-classified points were randomly selected as the locations for vertical checkpoints from each vegetation type (600 total vertical checkpoints). For context, the ASPRS (2015) accuracy reporting standards for geospatial data recommend a minimum of 20 vertical checkpoints per vegetation type, located away from vertical artifacts (e.g., rocks or fallen dead trees) and terrain with abrupt vertical changes. In anticipation of being unable to survey some vertical checkpoints, 100 random vertical checkpoints were chosen per vegetation type in order to ensure at least 20 would be surveyed in the field.

2.4.3.2 Vegetation height extraction

To extract tree, grass, and shrub heights from the LiDAR data, we developed a digital canopy height model (DCHM). First, the ground-classified points were used to make a digital terrain model (DTM). The chosen DTM resolution was 0.30 m because the point cloud contained an average ground point spacing of 0.30 m. To compute the DTM, the ground points were interpolated with minimum binning – each 0.30 m cell was assigned the minimum elevation value of the points found within its extent. Natural neighbor interpolation was then used to compute the elevation values of cells without points. Then, all of the points (ground and non-ground) were interpolated into a 0.30 m digital surface model (DSM) using maximum binning with natural neighbor interpolation for empty cells. The 0.30 m DCHM was computed by

subtracting the DTM from the DSM. This general workflow is consistent with previous studies, with variations in interpolation methods (Persson et al., 2002; Gaveau & Hill, 2003; Zimble et al., 2003; Clark et al., 2004; Hirata, 2004; Maltamo et al. 2004; Suarez et al., 2005; Kwak et al., 2007; Glenn et al., 2011).

2.4.4 Accuracy assessment

A survey-grade real-time kinematic (RTK) GNSS (GPS + GLONASS) was used to obtain ground reference measurements for accuracy assessment. Due to a lack of existing survey monuments at the study site, precise point positioning (PPP) was performed to establish a control point. A Trimble R4 GNSS base receiver logged raw data over a single location for approximately five hours. The base receiver data was post-processed with the Canadian Spatial Reference System (CSRS) PPP online tool to obtain a precise location of the control point. Identical to LiDAR data acquisition, all RTK GNSS data points were collected in the Universal Transverse Mercator (UTM) Zone 11 North (11N), North American Datum of 1983 (NAD83) projection, with orthometric Canadian Geodetic Vertical Datum of 1928 (CGVD28) heights.

Seven GCPs were evenly distributed throughout the study site to georeference the LiDAR point cloud (Figure 2.4). The targets were composed of 1.2 x 1.2 m white corrugated plastic boards painted black in one quadrant, allowing the target centers to be detectable with LiDAR intensity data. The target centers were surveyed with the RTK GNSS. Special care was taken to avoid depressing the GCP center with the bottom of rover rod in order to measure the true elevation of the target center.

The horizontal accuracy of the LiDAR point cloud was assessed by distributing 30 targets evenly throughout the site (Figure 2.4). ASPRS (2015) recommends a minimum of 20 horizontal checkpoints. The targets were 0.4 m diameter discs composed of white corrugated cardboard, elevated 0.5 m above the surface on wooden stakes, and leveled. Disc centers were also surveyed with the RTK GNSS.

Figure 2.4 Location of RTK GNSS base station, ground control points, and horizontal checkpoints.

2.4.5 Reference data

The LiDAR data were collected on 02 June 2016. Field-based reference measurements of shrub and grass height were collected on 14-16 June 2016, and tree heights were measured on 22 June to 07 July 2016. Ground surface elevation reference measurements were collected on 05-21 August 2016.

2.4.5.1 Ground elevation

Following Hodgson and Bresnahan (2004), ground surface elevation reference measurements were collected at LiDAR point locations in order to eliminate vertical error due to interpolation. In areas of little or no canopy cover, an RTK GNSS stakeout survey was performed to measure elevation at the vertical checkpoints. A SECO topo shoe with a wide, flat, circular base was attached to the bottom of the RTK rover rod to avoid depressing the rod into the ground and underestimating elevation. All measurements were obtained within a 0.15 m planar distance of their respective LiDAR point. Within the coniferous tree areas, where canopy cover prohibited adequate satellite geometry for RTK GNSS collection, a Nikon DTM-522 Total Station was used to obtain 300 random elevation measurements with the intention that at least 20 of these measurements would be located within a 0.15 m planar distance of a LiDAR point. The 0.15 m threshold distance was chosen to remain consistent with the RTK GNSS and LiDAR point maximum separation distance.

2.4.5.2 Vegetation height

Standard forestry surveying techniques using trigonometric principles were applied to measure the heights of trees. By measuring the horizontal distance to the tree, the angle to the tree top, and the tree height below the horizontal measurement, the total height of the tree was calculated. The standard instrument for measuring the horizontal distance and tree-top angle is a hypsometer, however, the tree height measurement error of this instrument has been found to range from 0.3 m to 0.8 m (Persson et al., 2002; Hopkinson et al., 2005; Andersen et al., 2006; Wallace et al., 2014). Therefore, in this study, a Total Station was used to measure tree heights due to the superior angular and ranging accuracy. First, the Total Station was set up over a control point established with the RTK GNSS. A reflective prism was positioned by an assistant against the tree and its height was manually adjusted until its center was aligned horizontally to

the height mark on the Total Station. The Total Station operator acquired a laser distance measurement to the prism, while the assistant recorded the height of the prism above ground level with a steel tape measure. The angle of the Total Station when the telescope was aimed at the tree top was then recorded. In total, 74 coniferous and 48 deciduous tree heights were measured using this method.

Height measurements of grasses and shrubs were acquired with a steel tape measure, while the coordinates of each measurement were recorded by the RTK GNSS. For grasses, a 0.5 m diameter ring was randomly placed on the surface. The RTK rover rod was placed inside the ring, near the point of maximum plant height, and the distance from the ground surface to the top of the plant was measured. For shrubs, the RTK rover rod was placed next to the shrub and the distance from the ground surface to the top of the plant was measured. In total, 49 short grass patches, 75 tall grass patches, 84 short shrubs, and 63 tall shrubs were measured in the field.

2.4.6 Data analysis

2.4.6.1 Horizontal accuracy

To calculate horizontal accuracy, LiDAR points from the surface of the 30 horizontal checkpoints were isolated from the dataset. The center-point coordinate was calculated (i.e., interpolated) using the Circle Hough Transform as described in Csanyi and Toth (2007). The procedure involves tracing 0.4 m diameter circles around the center of each LiDAR point, resulting in areas of varying overlap, with the central target area having maximum (all circles) overlap. A 0.01 m accumulator array (i.e., grid) was then applied, with each cell value representing the amount of overlapping circles. The cells where all the circles overlapped were isolated, and the center of gravity (i.e., mean center) of the maximum overlap area was used as the data-derived target center. Csanyi and Toth (2007) used this Circle Hough Transform method to georeference LiDAR data, and found the calculated target center to be horizontally accurate within 0.05 to 0.10 m.

Of the 30 horizontal checkpoints, ten were removed from the analysis during two major steps. First, eight horizontal checkpoints were removed during the LiDAR point isolation because they contained an inadequate number of LiDAR points (i.e., < 5) or an inadequate spatial distribution of points (e.g., only one half of target contained points). Then, two horizontal checkpoints were removed during the 0.01 m accumulator array application. For these

checkpoints, the maximum overlap area did not contain all of the LiDAR point circles, suggesting inaccurate LiDAR point isolation.

The horizontal error at each of the 20 remaining horizontal checkpoints was computed as the planar distance between the RTK GNSS-measured center and the calculated center from the Circle Hough Transform method. As recommended by ASPRS (2015), error statistics used in this study included the root mean square error (RMSE) in the x-direction ($RMSE_x$) and y-direction ($RMSE_y$):

$$RMSE_{x,y} = \sqrt{\frac{1}{n}\sum_{i=1}^{n}(x, y_{i(LiDAR)} - x, y_{i(ref)})^2} \quad \text{[Eq.1]}$$

where $x, y_{i(LiDAR)}$ is the coordinate (x- or y-directions) of the ith horizontal checkpoint from the LiDAR data, $x, y_{i(ref)}$ is the reference coordinate (x- or y-directions) measured during the ground survey, and the total number of observations is represented by n. The horizontal linear RMSE in the radial direction that includes both x- and y-coordinate errors ($RMSE_r$) was also calculated:

$$RMSE_r = \sqrt{{RMSE_x}^2 + {RMSE_y}^2} \quad \text{[Eq.2]}$$

where $RMSE_x$ is the RMSE in the x-direction, and $RMSE_y$ is the RMSE in the y-direction.

2.4.6.2 Ground elevation accuracy

A total of 289 ground surface elevation reference measurements were surveyed in the field with the RTK GNSS. The 300 random reference measurements obtained with the Total Station were each spatially joined with the nearest LiDAR ground-classified point. If the reference measurement was within 0.15 m of a LiDAR point, the reference measurement was used in the analysis, resulting in 156 reference measurements from the Total Station. The threshold distance of 0.15 m was selected because this was the maximum planar distance between LiDAR and RTK GNSS reference points. In total, the 445 reference elevation measurements (z_{ref}) collected with the RTK GNSS and Total Station were compared against their respective LiDAR vertical

checkpoints (z_{LiDAR}) to calculate residuals ($z_{\text{LiDAR}} - z_{\text{ref}}$). According to ASPRS (2015) recommendations, the frequency distributions of residuals per vegetation type were considered in order to choose the appropriate statistic for reporting vertical accuracy. Due to non-normal distributions of residuals, vertical error for each vegetation type was calculated as the 95$^{\text{th}}$ percentile absolute error (Q_{95}):

$$Q_{95} = \left(A[n_w] + \left(n_d * (A[n_w + 1] - A[n_w])\right)\right) \quad \text{[Eq.3]}$$

where *A* is an array of the absolute values of the samples, indexed in ascending order from *1* to *N*, *A[i]* is the sample value of array *A* at index *i* (e.g., n_w or n_d), *i* is an integer between *1* and *N*, *n* is the rank of the observation that contains the 95$^{\text{th}}$ percentile, n_w is the whole number component of *n*, and n_d is the decimal component of *n* (ASPRS, 2015).

2.4.6.3 Vegetation height accuracy

Grass and shrub heights were extracted from the DCHM using the sample locations from the field measurements. The coordinates of trees from the Total Station measurements were used to make 1 m tree buffers. The maximum DCHM value within each 1 m tree buffer was extracted. In total, 74 coniferous trees, 48 deciduous trees, 49 short grasses, 75 tall grasses, 84 short shrubs, and 63 tall shrubs were analyzed. The field-derived reference height measurements (h_{ref}) were compared against the respective LiDAR-derived heights (h_{LiDAR}) to calculate residuals ($h_{\text{LiDAR}} - h_{\text{ref}}$). Due to non-normal distributions of residuals, vegetation height error for each vegetation type was calculated as the 95$^{\text{th}}$ percentile absolute error (Q_{95}).

2.5 Results and discussion

2.5.1 Horizontal accuracy

Table 2.3 shows basic descriptive statistics for the x-direction, y-direction, and radial residuals, with histograms shown in Figure 2.5. The minimum and maximum absolute errors of the x- and y-direction residuals were 0.03 m and 0.05 m, respectively. The median error for the x- and y-directions was 0.00 m, suggesting no systematic bias in either direction. This is further demonstrated in Figure 2.5, which shows the radial error and offset direction of each LiDAR-derived horizontal checkpoint center. There is no consistent offset direction among the 20

checkpoints or among checkpoints following the same flight line (oriented southwest to northeast). The minimum and maximum radial errors were 0.01 m and 0.06 m, respectively.

Table 2.3 UAV-LiDAR horizontal residual error statistics in x-, y-, and radial directions.

Horizontal error component	Median error (interquartile range) (m)	Minimum error, maximum error (m)
x-direction	0.00 (0.02)	-0.03, 0.04
y-direction	0.00 (0.04)	-0.05, 0.04
radial	0.02 (0.02)	0.01, 0.06

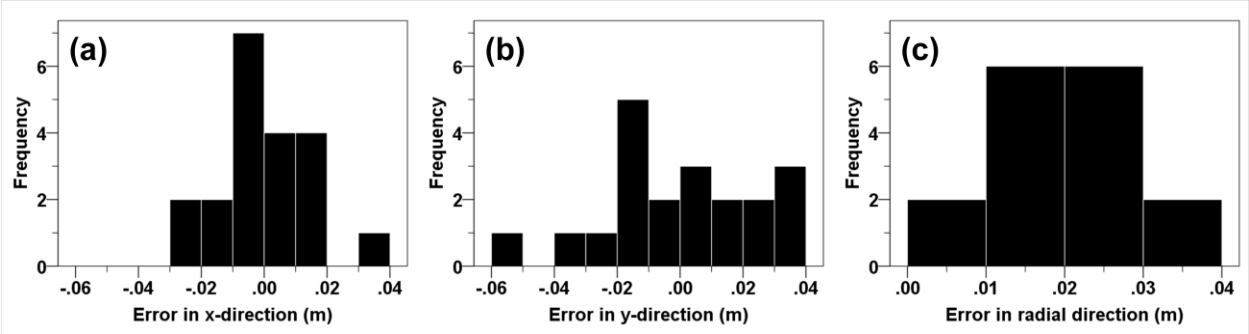

Figure 2.5 UAV-LiDAR horizontal checkpoint residuals (a) in the x-direction, (b) in the y-direction, and (c) in the radial direction that includes the x- and y-coordinate errors.

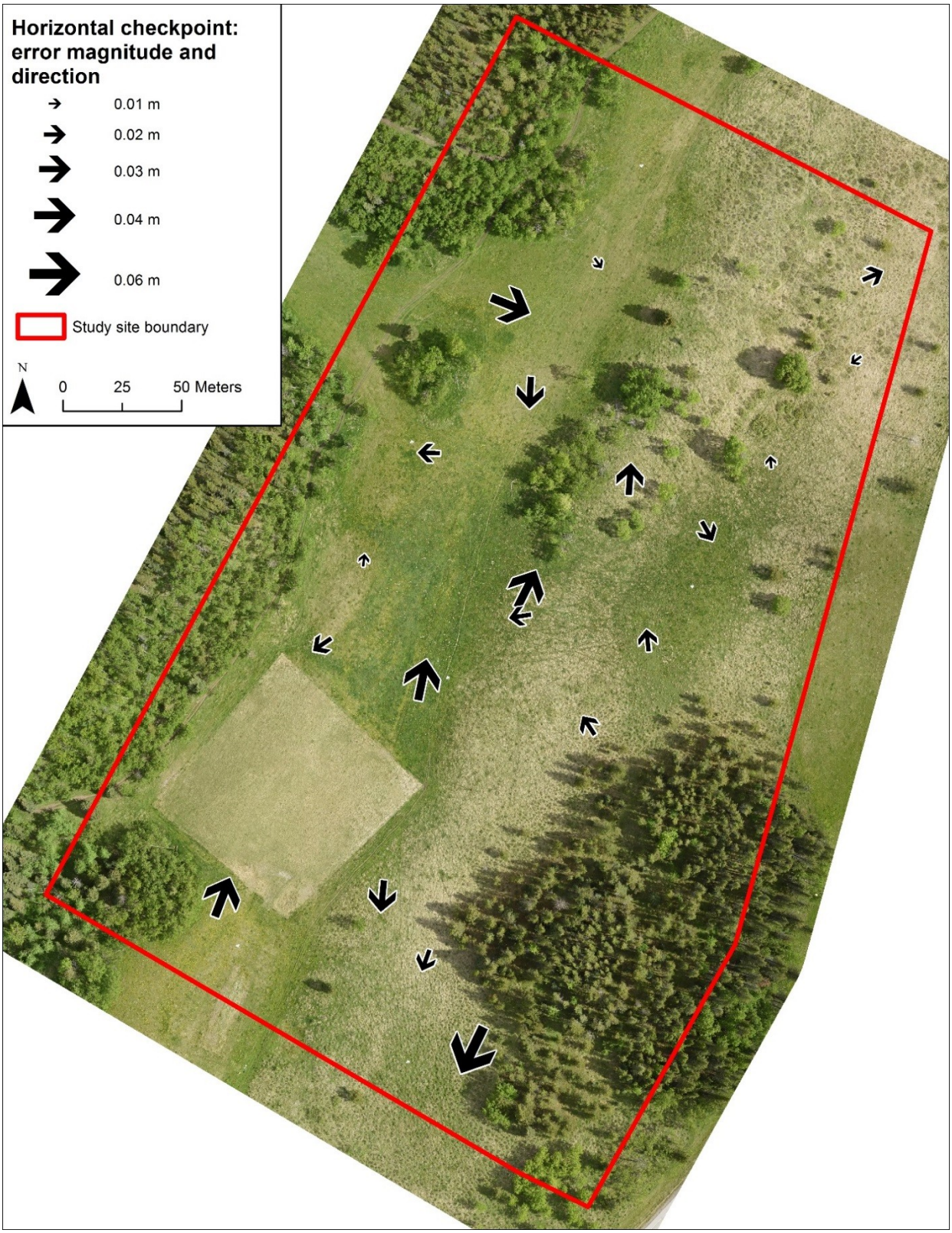

Figure 2.6 UAV-LiDAR horizontal checkpoint residuals: offset distances and directions of the Circle Hough Transform-derived target centers relative to field-surveyed target centers.

Following ASPRS (2015), the horizontal accuracy class, $RMSE_x$, $RMSE_y$, $RMSE_r$, and horizontal accuracy at the 95% confidence level were calculated using the 20 checkpoints (Table 2.4). Based on the 20 checkpoints, the LiDAR data meet the requirements of a 0.02 m horizontal accuracy class, with $RMSE_x$ and $RMSE_y$ of 0.02 m and $RMSE_r$ of 0.03 m, and a horizontal accuracy of 0.05 m at the 95% confidence level. To extrapolate the general implication of the $RMSE_r$, the potential vertical error caused by the horizontal error ($RMSE_r$) can be calculated (Hodgson et al., 2005):

$$Elevation\ Error = \tan(\theta) * RMSE_r \quad \text{[Eq. 4]}$$

where θ is the mean slope (degrees) of the study site, and $RMSE_r$ is the LiDAR horizontal error in the radial direction. For this particular study site, which contains a mean slope of 3°, the 0.03 m $RMSE_r$ contributes a negligible vertical error (i.e., 0.002 m) to the dataset. For study sites with more severe slopes of, for example, 45° (e.g., geologic outcrops, mountainous terrain), the contributed vertical error would be 0.03 m.

Table 2.4 UAV-LiDAR horizontal error statistics as recommended by ASPRS (2015) Table 7.1.

Horizontal accuracy class	$RMSE_x$ and $RMSE_y$ (m)	$RMSE_r$ (m)	Horizontal accuracy at 95% confidence level (m)
0.02-m	≤ 0.02	≤ 0.03	≤ 0.05

2.5.1.1 Comparison with previous UAV-LiDAR studies

Wallace et al. (2012) assessed the horizontal and vertical accuracies of UAV-LiDAR data using a multi-rotor platform and Ibeo LUX laser scanner from 50 m AGL. A total of 130 high reflectivity checkpoints distributed throughout the study site were used in the accuracy assessment. The centers of the checkpoints were surveyed with dual frequency differential GPS. LiDAR points that reflected off the checkpoints were identified using pulse width information. Each checkpoint's LiDAR point coordinates were averaged, and the LiDAR-derived checkpoint center x- and y-coordinates were compared with the field-surveyed coordinates. The horizontal RMSE based on 130 checkpoints was 0.60 m, which is 20 times higher than the horizontal

RMSE of 0.03 m based on 20 horizontal checkpoints in our study. A factor contributing to this difference may be our smaller sample size. However, the horizontal RMSE reported in Wallace et al. (2012) consisted of eight transects, each containing 15-18 checkpoints. The horizontal RMSEs of each of these transects ranged from 0.40 m to 0.85 m, which are well above 0.03 m. Additionally, Wallace et al. (2016) used the same method to measure the horizontal RMSE of UAV-LiDAR data acquired from 30 m AGL, also using the same UAV-LiDAR system. Based on 10 checkpoints, they calculated a horizontal RMSE of 0.42 m. Another factor that may have contributed to the difference is the method used to derive the checkpoint center coordinates from the LiDAR points. Wallace et al. (2012, 2016) averaged the x-, y-, and z-coordinates of the LiDAR points, which can lead to horizontal error when there is an uneven distribution of LiDAR points on the checkpoint (Wallace et al., 2012). Another important difference is that we used ground control targets for georeferencing our data, while Wallace et al. (2012, 2016) used direct georeferencing. Additional factors that may contribute to different horizontal RMSEs include differences in platform, componentry, flight and data acquisition parameters, and post-processing.

2.5.2 Ground elevation accuracy

2.5.2.1 LiDAR point cloud attributes

The resulting LiDAR point cloud contained a total of 5,399,697 point records, of which 1,086,968 (20%) were classified as ground and the rest (4,312,729, 80%) as vegetation. A majority of the points (58%) were from single-return pulses. Of the points that were part of multiple-return pulses (42%), 53% were 1st returns, 38% were 2nd returns, 9% were 3rd returns, 1% were 4th returns, and 0.1% were 5th returns. The average point density and spacing was 57 pts/m^2 and 0.13 m, respectively. The average ground point density and spacing was 11 pts/m^2 and 0.30 m, respectively (Table 2.2). Figure 2.7 shows the spatial distribution of ground point density. The treed areas, particularly the group of conifers in the southern corner of the study site, contained numerous ground point gaps, which accounted for approximately 7% of the coniferous tree area. To further investigate these gaps, the ground points were colored by scan angle (the angle off nadir that the laser pulse was emitted) (Figure 2.8). The dark green points (0° scan angle) represent the four flight lines oriented southwest to northeast. Within the conifers, the moderate to high scan angle (i.e., 20-40°) areas appear to contain fewer ground point gaps

than the nadir to low scan angle (< 20°) areas. These differences could be due to a greater ground point density in high scan angle areas from flight strip overlap. Additionally, at high scan angles, the laser pulse may be less obstructed by vegetation, whereas at nadir and low scan angles, the laser pulse must vertically pass through a tree, and often even the last return does not reach the ground. In Figure 2.9, the ground points are colored by the pulse return number. Points from 2nd, 3rd, 4th, and 5th returns are present mostly in the treed areas. Large ground point gaps encompassing entire tree crowns appear to be associated with nadir to low scan angles.

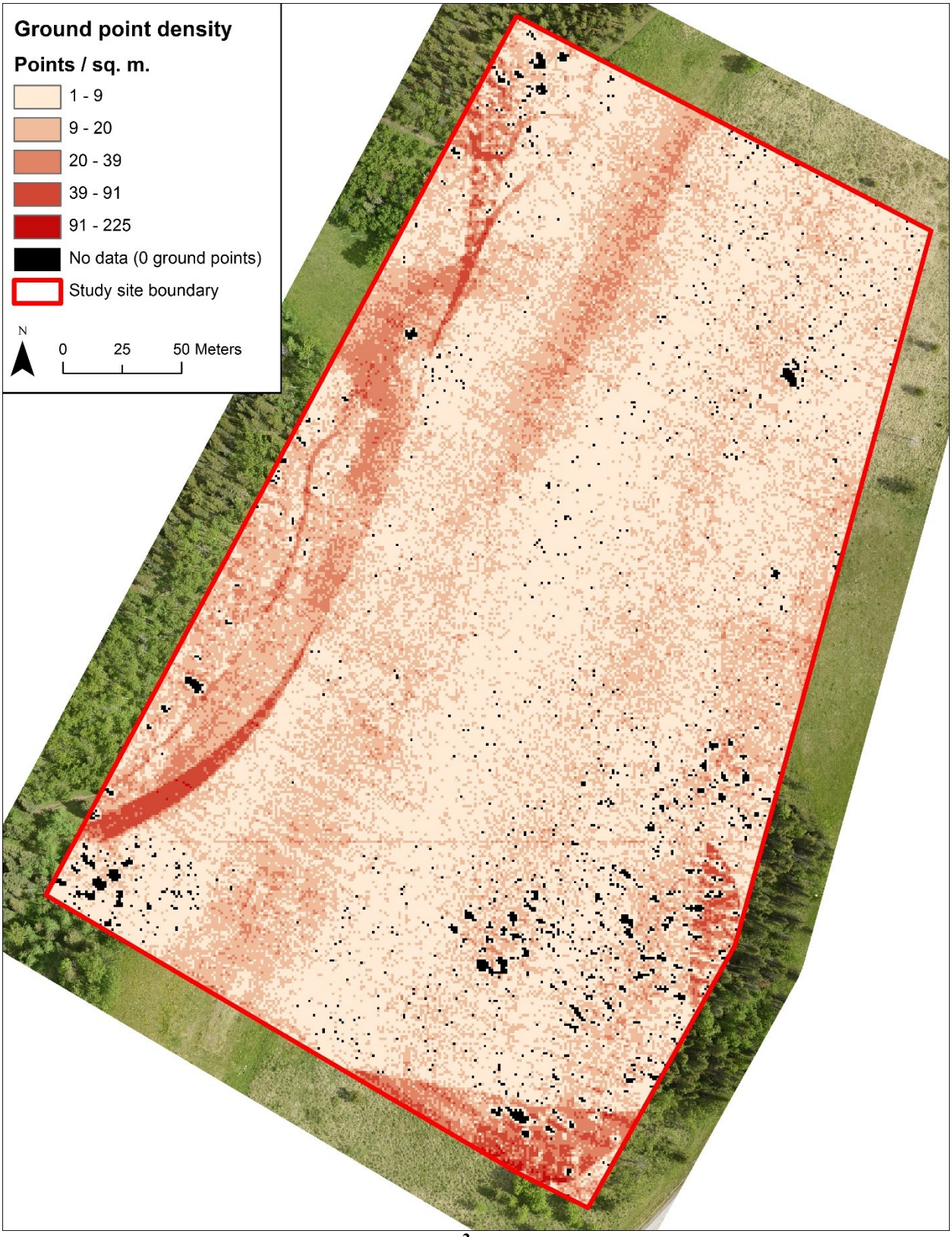

Figure 2.7 UAV-LiDAR point density (pts/m^2) of ground-classified points. Data gaps (no ground classified points) are shown in black.

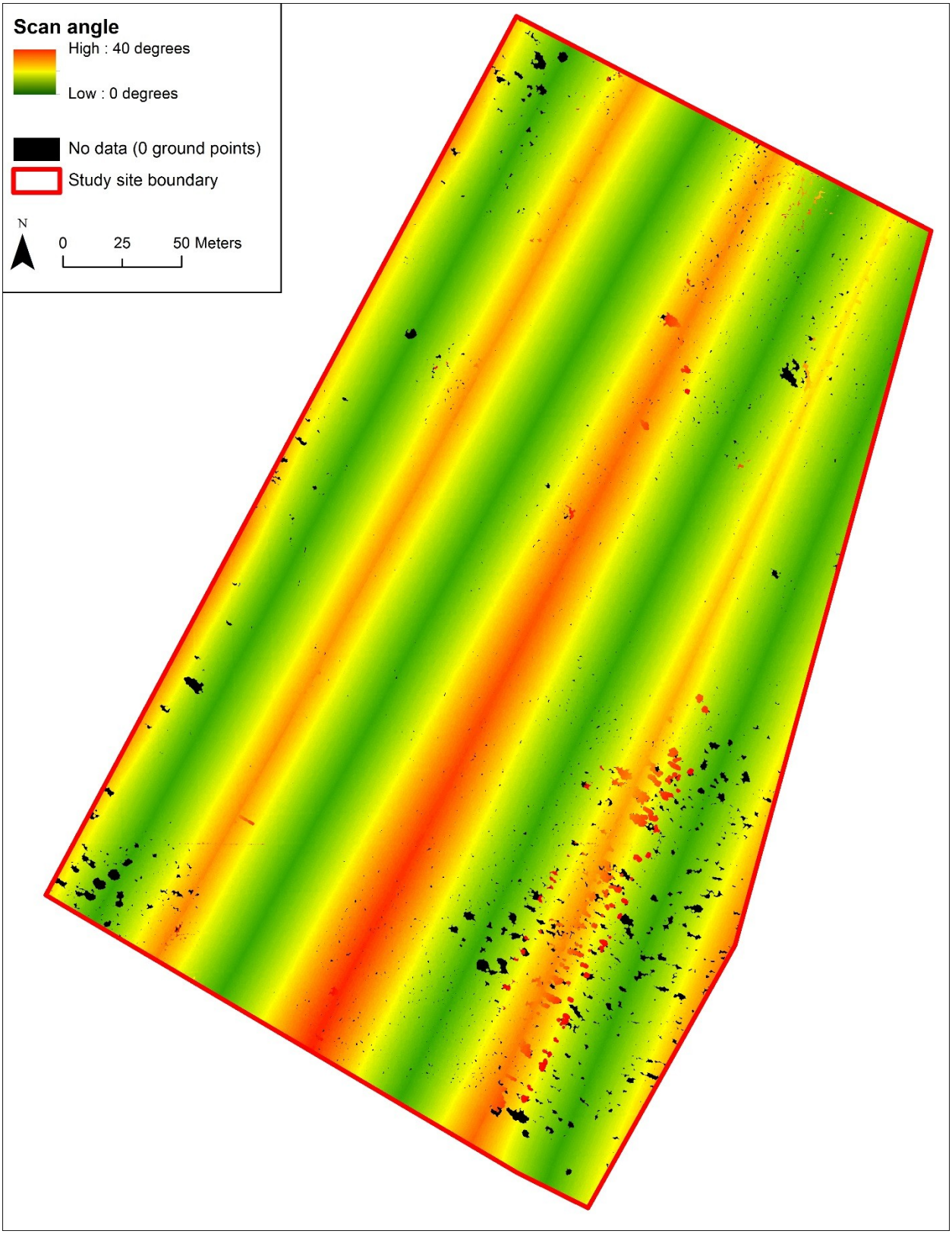

Figure 2.8 UAV-LiDAR ground-classified points colored by scan angle.

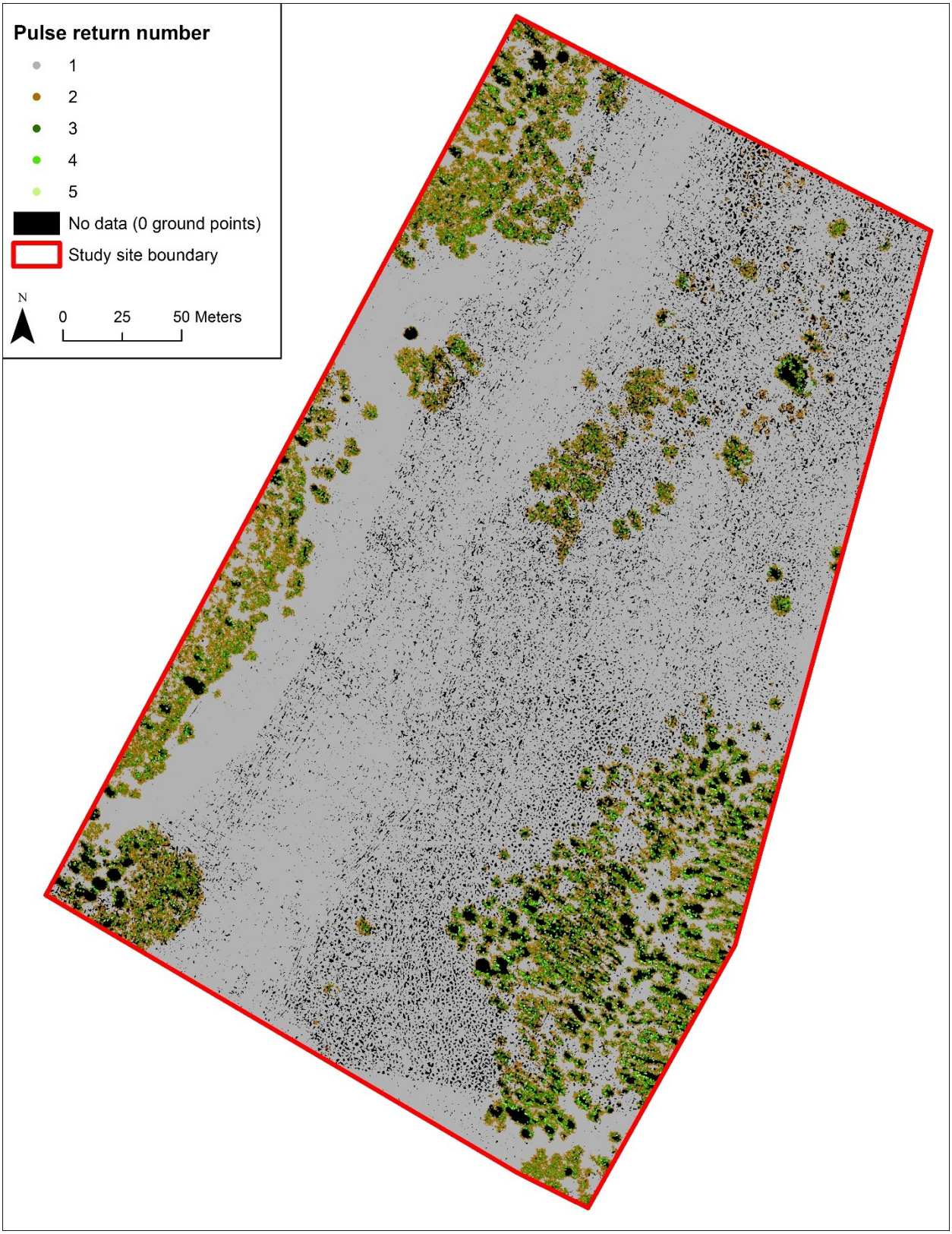

Figure 2.9 UAV-LiDAR ground-classified points colored by return number.

2.5.2.2 Vertical errors of LiDAR points

The elevations of the 445 LiDAR points randomly selected for the stakeout survey were compared against field-measured elevations, and residuals ($z_{\text{LiDAR}} - z_{\text{ref}}$) were calculated for each vegetation type (Table 2.5). The residuals ranged from -0.07 m for coniferous and deciduous trees to 0.15 m for deciduous trees. Median errors among vegetation types ranged from 0.00 m to 0.04 m, with coniferous trees and short grass containing 0.00 m median errors. Since most of the median errors were positive, a One-Sample Sign test (α level of 0.05) was performed for all the data combined and for each vegetation type to determine if the median residual was significantly greater than 0.00 m. This test was used to determine if the LiDAR data had a tendency to overestimate ground elevation. The *p*-values from the One-Sample Sign test (Table 2.5) indicated that the median residuals of all classes, except coniferous trees and short grass, were significantly greater than 0.00 m. The positive median residuals demonstrate a tendency for the LiDAR system to overestimate ground elevation, which could be due to: (i) dense vegetation preventing the laser pulse from reaching the ground surface, and (ii) point classification commission errors (i.e., points from vegetation that were misclassified as ground points).

Following ASPRS (2015), we examined the frequency distributions of the residuals before selecting the appropriate vertical accuracy reporting statistic. A Shapiro-Wilk test (α level of 0.05) and a visual inspection of the histograms, normal Q-Q plots, and box plots indicated that not all vegetation types had normal distributions of residuals (Figure 2.10). Therefore, as recommended by ASPRS (2015), vertical accuracy was calculated as the 95$^{\text{th}}$ percentile absolute error (Q_{95}), overall and per vegetation type (Table 2.5). Overall, Q_{95} was 0.08 m, and vegetation type-specific Q_{95} ranged from 0.06 m (coniferous trees) to 0.11 m (deciduous trees). Following ASPRS (2015), the vertical accuracy class and vegetated vertical accuracy (VVA) at the 95% confidence level were calculated. Based on the 445 vertical checkpoints, the LiDAR data meet the requirements of a 0.08 m vertical accuracy class and contain a 0.24 m VVA at the 95% confidence level.

Table 2.5 UAV-LiDAR vertical error statistics. The One-Sample Sign test (α level of 0.05) contained a null hypothesis that the median residual equals 0.00 m, and an alternative hypothesis that the median residual is greater than 0.00 m – bold *p*-values indicate the median residual is significantly greater than 0.00 m.

Vegetation type	*n*	Median error (interquartile range) (m)	*p*-value (95% confidence interval) of One-Sample Sign test	Min. error, max. error (m)	95th percentile absolute error (m)
All (combined)	445	0.01 (0.05)	**0.0000** (0.0100, 0.0200)	-0.07, 0.15	0.08
Coniferous trees	156	0.00 (0.04)	0.3970 (0.0000, 0.0100)	-0.07, 0.08	0.06
Deciduous trees	56	0.03 (0.06)	**0.0004** (0.0124, 0.0428)	-0.07, 0.15	0.11
Short grass	57	0.00 (0.04)	0.4468 (-0.0080, 0.0137)	-0.05, 0.10	0.07
Tall grass	62	0.02 (0.04)	**0.0000** (0.0157, 0.0272)	-0.03, 0.10	0.08
Short shrubs	57	0.04 (0.03)	**0.0000** (0.0310, 0.0483)	-0.03, 0.14	0.09
Tall shrubs	57	0.03 (0.04)	**0.0000** (0.0183, 0.0353)	-0.02, 0.10	0.09

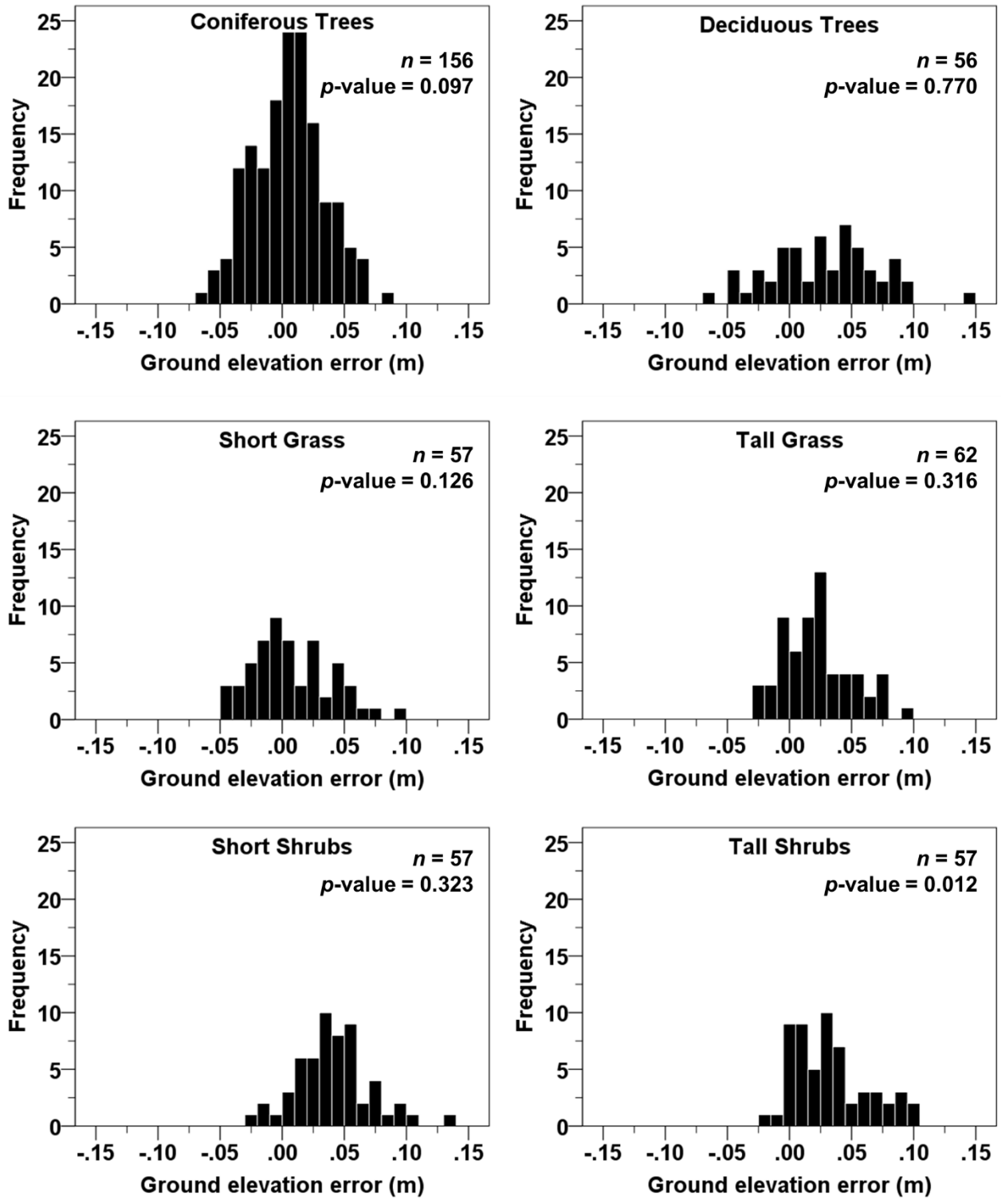

Figure 2.10 Histograms of UAV-LiDAR vertical error and *p*-values from a Shapiro-Wilk normality test (α level of 0.05) for each vegetation type.

2.5.2.3 Differences between vegetation types

The median residuals of each vegetation type were compared to those of other vegetation types in order to determine if they differed significantly. First, due to the non-normality of residuals in some vegetation types (Figure 2.10), a non-parametric Levene's test (α level of 0.05) was used to inspect equality of variance among the residuals in each vegetation type pair in order to determine which median-comparison hypothesis test to perform. The *p*-values from the non-parametric Levene's test indicated inequality of variance (heteroscedasticity) among the residuals of several vegetation type pairs. Due to the non-normality and heteroscedasticity, a Mood's Median test (α level of 0.05) was performed on vegetation type pairs in order to determine if median residuals between vegetation type pairs were significantly different. The *p*-values from the Mood's Median test (Table 2.6) indicate significant differences in median residuals between: coniferous and deciduous trees, short and tall grass, short and tall shrubs, and numerous tree/grass/shrub combinations. The class pairs that did not exhibit significantly different median residuals were: coniferous trees and short grass, deciduous trees and tall grass, deciduous trees and short shrubs, deciduous trees and tall shrubs, and tall grass and tall shrubs. Most of these *p*-values were 0.344 and under. The vegetation pairs with higher *p*-values were deciduous trees and short shrubs (0.777) and deciduous trees and tall shrubs (0.780). The ground cover underneath the deciduous trees is important to consider – many vertical checkpoints located under deciduous trees coincided with short and tall shrubs.

Table 2.6 *p*-values and 95% confidence intervals of Mood's Median test (α level of 0.05) performed on the UAV-LiDAR median vertical residuals of vegetation type pairs. The Mood's Median test contained a null hypothesis that median residuals of the two vegetation types are equal, and an alternative hypothesis that there is a difference between the median residuals – bold *p*-values indicate the median vertical residuals significantly differ between the two vegetation types.

Vegetation type	Coniferous trees	Deciduous trees	Short grass	Tall grass	Short shrubs
Deciduous trees	**0.002** (-0.042,-0.014)				
Short grass	0.344 (-0.011, 0.007)	**0.006** (0.012, 0.047)			
Tall grass	**0.003** (-0.026,-0.016)	0.277 (-0.006, 0.024)	**0.013** (-0.032, -0.008)		
Short shrubs	**0.000** (-0.047,-0.032)	0.777 (-0.027, 0.008)	**0.000** (-0.053, -0.024)	**0.000** (0.007, 0.030)	
Tall shrubs	**0.000** (-0.034,-0.020)	0.780 (-0.012, 0.018)	**0.003** (-0.038, -0.015)	0.170 (-0.015, 0.003)	**0.039** (0.001, 0.024)

2.5.2.4 Comparison with piloted airborne LiDAR

Hodgson & Bresnahan (2004) performed a vertical accuracy assessment of LiDAR data obtained from a piloted aircraft survey of different land cover/vegetation types. Their data were acquired from 1207 m AGL during leaf-off conditions. They used a similar methodology by locating LiDAR points, measuring their elevation with an RTK GNSS, and calculating vertical RMSEs. They examined several different vegetation types: evergreen trees, deciduous trees, low grass, high grass, and brush/low trees. All of these vegetation types appear to be broadly comparable to the classes examined in our study, but with recognized differences in structure (e.g., Lodgepole Pine vs. Evergreen). We assume that their brush/low tree class is similar to our short and tall shrub classes. As shown in Table 2.7, our data produced higher vertical accuracies, as represented by the 95th percentile absolute errors. For each vegetation type, the RMSE values in Hodgson & Bresnahan's (2004) study were 2-3 times higher than the 95th percentile absolute errors of our UAV-LiDAR data. Factors likely contributing to the higher vertical accuracy of the UAV-LiDAR data include the lower (i.e., by 1,147 m) flying altitude of the UAV-LiDAR system, a lower scanning range, smaller footprint size, and higher point density to increase the probability of passing through breaks in canopy.

Table 2.7 Vertical error comparison between UAV-LiDAR and piloted LiDAR (Hodgson & Bresnahan, 2004).

	UAV-LiDAR		**Piloted LiDAR (Hodgson & Bresnahan, 2014)**	
Vegetation type	***n***	**95th percentile absolute error (m)**	***n***	**RMSE (m)**
Coniferous trees	156	0.06	119	0.17
Deciduous trees	56	0.11	82	0.26
Short grass	57	0.07	137	0.23
Tall grass	62	0.08	98	0.19
Shrubs	57	0.09	98	0.23

2.5.2.5 Comparison with previous UAV-LiDAR studies

As described in Section 2.5.1.1, Wallace et al. (2012) used 130 checkpoints to assess the horizontal and vertical accuracy of UAV-LiDAR data acquired from 50 m AGL. From the LiDAR points that reflected off each target, the mean elevation was calculated and compared against the field-measured checkpoint center elevation. Using this method, Wallace et al. (2012)

calculated a vertical RMSE of 0.19 m. Wallace et al. (2016) applied the same method to measure the vertical RMSE of UAV-LiDAR data acquired from 30 m AGL, also using the same UAV-LiDAR system. Using 10 targets, they calculated a vertical RMSE of 0.17 m. Our data, acquired from 60 m AGL, had an overall vertical Q_{95} of 0.08 m, which was based on 445 checkpoints co-located with actual LiDAR points in vegetated terrain. Wallace et al. (2012, 2016) used artificial targets and averaged the elevation values of LiDAR points to obtain the checkpoint elevation, which is prone to error with an uneven distribution of points and unleveled targets. Again, it is important to note that other factors (mentioned in Section 2.5.1.1) likely contributed to this difference in overall vertical error.

2.5.2.6 Comparison with UAV-SfM

Dandois and Ellis (2013) assessed the vertical accuracy of UAV-SfM in vegetated terrain. They calculated DTM error under forest canopy in leaf-on conditions, with vertical RMSEs ranging from 0.59 to 0.61 m. In coniferous and deciduous trees, our 95th percentile absolute errors were 0.06 m and 0.11 m, respectively. Jensen and Mathews (2016) calculated the vertical accuracy of UAV-SfM in shrubby and treed terrain with 16 vertical checkpoints, and calculated a median error of 0.10 m. Our comparable median vertical errors were 0.00 m (coniferous trees), 0.03 m (deciduous trees), 0.04 m (short shrubs), and 0.03 (tall shrubs).

2.5.3 Vegetation height accuracy

2.5.3.1 Errors of LiDAR-based vegetation heights

Vegetation heights measured in the field ranged from: (i) coniferous trees (3.79 m to 23.24 m), (ii) deciduous trees (8.18 m to 17.33 m), (iii) short grass (0.03 m to 0.30 m), (iv) tall grass (0.31 m to 1.13 m), (v) short shrubs (0.40 m to 0.99 m), and (vi) tall shrubs (1.03 m to 1.83 m). Residuals calculated from the difference in vegetation height between the UAV-LiDAR DCHM and field measurements ($h_{\mathrm{LiDAR}} - h_{\mathrm{ref}}$) are presented for each vegetation type in Table 2.8. The residuals ranged from -13.38 m (coniferous trees) to 5.97 m (short shrubs). However, the residual of -13.38 m occurred near the edge of LiDAR data collection, where even the highest scan angle (i.e., 40°) could not capture the entire tree. Median errors among vegetation types ranged from -0.20 m (short grass) to -0.48 m (deciduous trees). Since all of the median errors were negative, a One-Sample Sign test (α level of 0.05) was performed for each vegetation type to determine if

the median was significantly less than 0.00 m. This test was used to determine if the LiDAR data had a tendency to underestimate vegetation height. The *p*-values of the One-Sample Sign test (Table 2.8) indicate that the medians of all classes were significantly less than 0.00 m. The negative median residuals demonstrate a tendency for the LiDAR data to underestimate vegetation height, which could be caused by: (i) the laser pulse missing the tree tops or grass/shrub field measurement locations, and/or (ii) an overestimation of the ground surface elevation in the DTM. As was done with vertical accuracy reporting, we inspected the frequency distributions of the residuals before selecting the appropriate vegetation height accuracy reporting statistic. A Shapiro-Wilk test (α level of 0.05) and a visual inspection of the histograms, normal Q-Q plots, and box plots indicated that all vegetation types had non-normal distributions of residuals (Figure 2.11). Therefore, vegetation height accuracy was calculated as the 95th percentile absolute error (Q_{95}) overall and per vegetation type. The overall vegetation height Q_{95} was 1.17 m, and ranged from 0.28 m for short grass to 3.31 m for coniferous trees. This Q_{95} range (i.e., 3.03 m) is much larger than the vertical Q_{95} range among vegetation types (i.e., 0.05 m). This large range highlights the importance of considering vegetation height error separately for each vegetation type instead of using a combined approach, as the overall Q_{95} of 1.17 m grossly misrepresents lower errors (especially short grasses) and larger errors (especially coniferous trees). Importantly, the vegetation height Q_{95} values of some vegetation types were as large or exceed the maximum height of the vegetation type (i.e., short grass and short shrubs), which may not provide practitioners the necessary confidence in measurement. The magnitude of the Q_{95} values per vegetation type should be considered before employing UAV-LiDAR to measure vegetation height.

Table 2.8 UAV-LiDAR vegetation height error statistics. The One-Sample Sign test (α level of 0.05) contained a null hypothesis that the median residual equals 0.00 m, and an alternative hypothesis that the median residual is less than 0.00 m – bold p-values indicate the median residual is significantly less than 0.00 m.

Vegetation type	*n*	Median error (interquartile range) (m)	*p*-value (95% confidence interval) of One-Sample Sign test	Min. error, max. error (m)	95th percentile absolute error (m)
All (consolidated)	393	-0.34 (0.30)	**0.0000** (-0.3659, -0.3078)	-13.38, 5.97	1.17
Coniferous trees	74	-0.41 (0.41)	**0.0000** (-0.5037, -0.3485)	-13.38, 3.76	3.31
Deciduous trees	48	-0.48 (0.57)	**0.0000** (-0.6078, -0.3671)	-2.76, 0.80	1.91
Short grass	49	-0.20 (0.07)	**0.0000** (-0.2261, -0.1875)	-0.30, -0.03	0.28
Tall grass	75	-0.37 (0.16)	**0.0000** (-0.4027, -0.3456)	-0.99, -0.07	0.72
Short shrubs	84	-0.30 (0.27)	**0.0000** (-0.3467, -0.2743)	-0.77, 5.97	0.67
Tall shrubs	63	-0.41 (0.56)	**0.0000** (-0.5273, -0.2638)	-1.38, 2.92	1.34

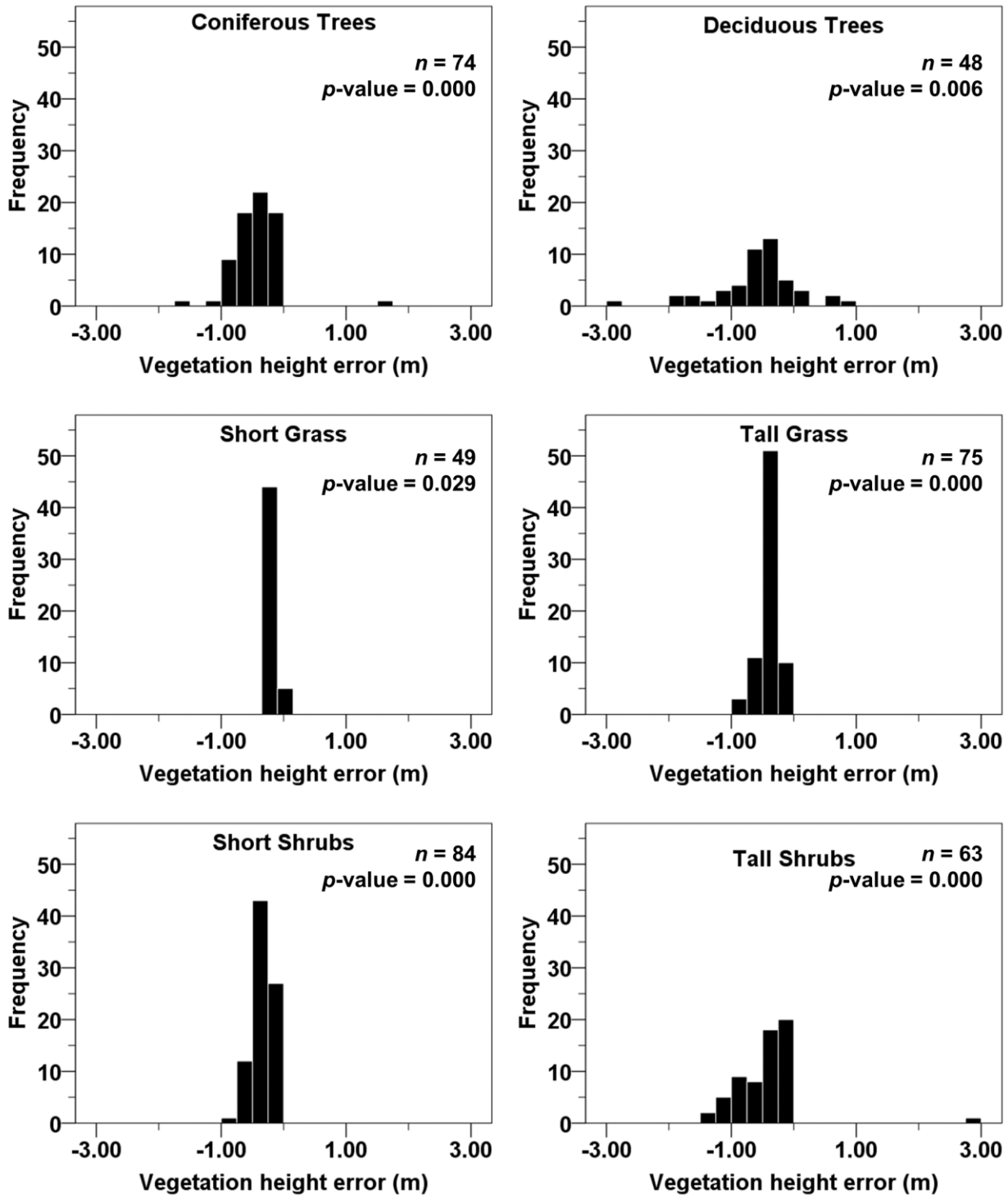

Figure 2.11 UAV-LiDAR vegetation height error histograms and p-values from a Shapiro-Wilk normality test (α level of 0.05) for each vegetation type.

2.5.3.2 Differences between vegetation types

The median residuals of each vegetation type were compared to those of other vegetation types in order to determine if they significantly differ. First, due to the non-normality of residuals in some vegetation types (Figure 2.11), a non-parametric Levene's test (α level of 0.05) was used to inspect equality of variance among the residuals in each vegetation type pair in order to determine which median-comparison hypothesis test to perform. The *p*-values from the non-parametric Levene's test indicated inequality of variance (heteroscedasticity) among the residuals of most vegetation type pairs. Due to the non-normality and heteroscedasticity, a Mood's Median test (α level of 0.05) was performed on vegetation type pairs. The *p*-values from the Mood's Median test (Table 2.9) indicate significant differences in median residuals for all vegetation type pairs with the exception of coniferous and deciduous trees, coniferous trees and tall shrubs, deciduous trees and tall shrubs, and tall grass and short shrubs. Of these, the three highest *p*-values were associated with deciduous trees and tall shrubs (0.286), coniferous trees and deciduous trees (0.459), and coniferous trees and tall shrubs (0.926). These high *p*-values can be explained by the similar median errors and similarly large interquartile ranges of coniferous trees, deciduous trees, and tall shrubs. Vegetation height errors did not significantly differ between coniferous trees, deciduous trees, and tall shrubs.

Table 2.9 *p*-values and 95% confidence intervals of Mood's Median test (α level of 0.05) performed on the UAV-LiDAR median vegetation height residuals of vegetation type pairs. The Mood's Median test contained a null hypothesis that median residuals of the two vegetation types are equal, and an alternative hypothesis that there is a difference between the median residuals – bold *p*-values indicate the median vegetation height residuals significantly differ between the two vegetation types.

Vegetation type	Coniferous trees	Deciduous trees	Short grass	Tall grass	Short shrubs
Deciduous trees	0.459 (-0.127, 0.190)				
Short grass	**0.000** (-0.299, -0.131)	**0.000** (-0.336, -0.147)			
Tall grass	0.219 (-0.145, 0.032)	0.160 (-0.193, 0.013)	**0.000** (0.128, 0.186)		
Short shrubs	**0.004** (-0.210, -0.019)	**0.004** (-0.254, -0.037)	**0.000** (0.067, 0.136)	**0.003** (0.019, 0.096)	
Tall shrubs	0.926 (-0.142,0.137)	0.286 (-0.187, 0.113)	**0.000** (0.134, 0.285)	0.232 (-0.030,0.140)	**0.036** (0.022, 0.201)

2.5.3.3 Comparison with piloted airborne LiDAR

To compare the vegetation height error of the UAV-LiDAR DCHM to that of LiDAR data obtained with piloted aircraft, we considered the results of Gaveau & Hill (2003) and Hopkinson et al. (2005). Gaveau & Hill (2003) found mean errors of -2.12 m for trees (n = 39) compared to our median tree height errors of -0.41 m (coniferous trees) and -0.48 m (deciduous trees). Hopkinson et al. (2005) found mean DCHM errors of -0.04 m for grasses (n = 31) compared to our median grass height errors of -0.20 m (short grass) and -0.37 m (tall grass). Gaveau & Hill (2003) found mean errors of -1.02 m for shrubs (n = 43) and Hopkinson et al. (2005) found mean errors of -0.39 m for low shrubs (n = 44), and -1.09 m for tall shrubs (n = 12). For comparison, our median shrub height errors were -0.30 m (short shrubs) and -0.41 m (tall shrubs). In general, the tree and shrub height errors show improvement with UAV-LiDAR compared to the piloted LiDAR DCHMs. The higher point density associated with UAV-LiDAR increases the probability of detecting tree and shrub tops (Lin et al., 2011; Wallace et al., 2011, 2012; 2014). However, the grass height errors are higher in the UAV-LiDAR DCHM, which was unexpected. Other factors may include the higher vertical accuracy of UAV-LiDAR relative to piloted airborne LiDAR.

2.5.3.4 Comparison with previous UAV-LiDAR studies

Wallace et al. (2014) calculated the tree height error of UAV-LiDAR data acquired from 40 m AGL with an aircraft velocity of 2.8 m/s. They measured 248 single-species trees distributed among six plots with mean tree heights ranging from 5.71 m to 8.93 m. The tree height RMSE of the UAV-LiDAR data relative to field-measured heights was 0.52 m. Using the same UAV-LiDAR system, Wallace et al. (2016) calculated the tree height error of LiDAR data acquired from 30 m AGL with a point density of 174 pts/m^2. The authors measured 122 single-species tree heights ranging from 4.7 m to 16.2 m, and the tree height RMSE was 0.92 m. Their lower tree height RMSEs relative to our tree height Q_{95} values (3.31 m for coniferous trees and 1.91 m for deciduous trees) may be due to their higher point density (i.e., their 174 pts/m^2 versus our 57 pts/m^2) from the lower flying altitude and velocity, contributing to the increased detection of tree tops and increased number of ground returns. Other factors contributing to an increased number of ground returns and thus lower tree height errors could be a result of differences in the foliage density and average tree spacing.

2.5.3.5 Comparison with UAV-SfM

In addition to UAV-LiDAR, Wallace et al. (2016) acquired UAV-borne RGB imagery for SfM-MVS. The resultant SfM-MVS data were used to extract 112 single-species tree heights ranging from 4.7 m to 16.2 m. Compared to field-measured heights, the tree height RMSE was 1.30 m. Zarco-Tejada et al. (2014) calculated tree height accuracy of UAV-SfM in an olive orchard containing 152 olive trees distributed in rows with heights ranging from 1.16 m to 4.38 m. The tree height RMSE was 0.35 m. Dandois and Ellis (2010) calculated the vegetation height accuracy of UAV-SfM using trees ranging in height from 4.30-33.60 m, with RMSEs of 3.28 m to 3.76 m. These results were similar to the UAV-LiDAR height Q_{95} values (i.e., 3.31 m for coniferous trees and 1.91 m for deciduous trees).

2.6 Conclusion

This study assessed the horizontal, vertical, and vegetation height accuracies of UAV-LiDAR data, and addressed whether the vertical and vegetation height errors varied among six vegetation types (coniferous trees, deciduous trees, short grass, tall grass, short shrubs, and tall shrubs). In the context of the 2015 ASPRS Positional Accuracy Standards for Digital Geospatial Data (ASPRS, 2015), the UAV-LiDAR data meet the requirements of a 0.02 m horizontal accuracy class and 0.08 m vertical accuracy class, based on a 0.05 m horizontal accuracy at the 95% confidence level and 0.24 m vegetated vertical accuracy (VVA) at the 95% confidence level. Per vegetation type, vertical accuracy was calculated as the 95th percentile absolute error (Q_{95}). Vertical Q_{95} values ranged from 0.06 (coniferous trees) to 0.11 m (deciduous trees), resulting in a 0.05 m range among the vegetation types. Vegetation height accuracy, on the other hand, varied greatly among the vegetation types, with Q_{95} values ranging from 0.28 m (short grass) to 3.31 m (coniferous trees). This large Q_{95} range should prompt practitioners to consider the Q_{95} for each vegetation type instead of the overall Q_{95}.

When compared to piloted LiDAR data from Hodgson and Bresnahan (2004), the vertical errors were 2-3 times lower in the UAV-LiDAR data per vegetation type. Tree and shrub height errors were lower for UAV-LiDAR as compared with other piloted LiDAR studies, but grass height error was higher for unknown reasons.

Compared to previous UAV-LiDAR and UAV-SfM studies (Wallace et al., 2012, 2014, 2016; Dandois & Ellis, 2013; Jensen & Mathews, 2016), our data achieved higher horizontal and

vertical accuracies for ground surface elevation. However, tree heights estimated from our data had higher error than the other UAV-LiDAR studies. We surmise this is due to the decreased point density from flying higher and faster than the previous studies. This lower point density decreased the likelihood of detecting tree tops, as well as penetrating vegetation to obtain ground surface measurements, resulting in higher tree height errors.

According to our results, UAV-LiDAR may be a better alternative to piloted LiDAR for small-area mapping applications where the accuracy of the ground surface elevation is paramount. However, for measuring vegetation height, the errors obtained in this study may be unacceptable for certain applications. To reduce vegetation height errors, a lower flying altitude and slower velocity will increase point density and the likelihood of recording plant tops and penetrating canopy to measure the ground surface. However, lower flight altitudes and speeds will decrease the areal data coverage, which is an important factor to consider when selecting the appropriate platform.

Chapter 3: UAV structure from motion photogrammetry: accuracy in vegetated terrain and comparison to UAV-LiDAR

3.1 Chapter abstract

This chapter examines the accuracy of ground surface elevation and vegetation height derived from the combination of multiview stereo images acquired by uninhabited / unmanned aerial vehicles (UAVs) and structure from motion (SfM) photogrammetry (UAV-SfM). UAV-SfM has created new capacity to develop high-resolution orthoimages and 3D topographic models for a range of professional and research applications. However, like all image-based remote sensing methods, UAV-SfM is prone to higher vertical error in areas covered by vegetation because the ground surface is not visible in stereo. Additionally, this error may vary considerably depending on vegetation structure and density. However, UAV-SfM vertical accuracy in different vegetation types is not well documented. To address this issue, this chapter evaluated the accuracy of a UAV-SfM dataset acquired during leaf-on conditions at a field site with six different vegetation types: trees (coniferous and deciduous), grasses (short and tall), and shrubs (short and tall). The accuracy of the dataset was determined from point-based measurements of ground surface elevation and vegetation height obtained with an RTK GNSS and a Total Station. Vertical checkpoint quantity/distribution and error reporting followed the 2015 ASPRS Positional Accuracy Standards for Digital Geospatial Data. This chapter also examined the differences in ground surface elevation and vegetation height errors between the UAV-SfM dataset and the UAV-LiDAR dataset from Chapter 2. Results shows that UAV-SfM ground surface elevation and vegetation height errors (as the 95th percentile absolute error, Q_{95}) were 0.17 m and 1.35 m, respectively. UAV-SfM ground surface elevation Q_{95} values ranged from 0.14 m (short grass) to 0.26 m (tall shrubs), with median errors significantly above 0.00 m for all vegetation types except coniferous trees. The UAV-SfM ground surface elevation errors are higher than the UAV-LiDAR errors for all vegetation types. UAV-SfM vegetation height Q_{95} values ranged from 0.22 m (short grass) to 2.58 m (coniferous trees), with all median errors significantly below 0.00 m. These vegetation height errors are lower than the UAV-LiDAR errors in coniferous trees, short grass, and tall grass, which likely reflect the higher point density in the UAV-SfM dataset. However, in forested areas the UAV-SfM dataset failed to resolve sub-

canopy tree structure, whereas the UAV-LiDAR dataset was able to consistently sample trunks and large branches.

3.2 Introduction

Structure from motion-multiview stereo (SfM-MVS) photogrammetric image processing has unlocked new capabilities for reconstructing landform geometry with very high spatial resolution and accuracy, particularly with application to the geosciences when imagery is acquired with an uninhabited / unmanned aerial vehicle (UAV). UAV-based SfM-MVS (hereafter UAV-SfM) combines multiview stereo imagery (acquired with consumer-grade digital cameras onboard UAVs) with computer vision and MVS algorithms to produce very high resolution digital elevation models (DEMs) and orthorectified mosaics, which have been shown to be accurate within 3 cm vertically and horizontally (Hugenholtz et al., 2016). Geoscience case studies have applied UAV-SfM to digitally reconstruct a variety of environments including: aeolian landforms (Hugenholtz et al., 2013), ultrafine fault zones (Johnson et al., 2014), fluvial environments (Tamminga et al., 2015), aggregate stockpiles (Hugenholtz et al., 2015), glaciers (Whitehead et al., 2013), landslides (Niethammer et al., 2012), and more. Due to the very high spatial resolution of the imagery acquired for UAV-SfM (typically 5 cm or finer), the generated geospatial data can be used for microtopographic studies (Carrivick et al., 2016).

With digital geospatial data, it is generally accepted that ground surface elevation errors will increase with the presence of vegetation. The 2015 American Society for Photogrammetry and Remote Sensing (ASPRS) Positional Accuracy Standards for Digital Geospatial Data (ASPRS, 2015) list two primary types of vertical accuracies that can be reported at the 95% confidence level: non-vegetated vertical accuracy (NVA) and vegetated vertical accuracy (VVA). NVA and VVA are both calculated using a multiplier – NVA uses 1.96, as vertical errors in non-vegetated terrain typically follow a normal distribution. Vertical errors in vegetated terrain, however, do not typically follow a normal distribution, and thus a higher multiplier of 3.00 is needed to estimate vertical accuracy at the 95% confidence level (ASPRS, 2015). This higher multiplier for calculating VVA at the 95% confidence level suggests that, universally, error is expected to be higher in vegetated terrain.

Previous studies using UAV-SfM have reported reduced vertical accuracy of digital terrain models (DTMs) due to the presence of vegetation (Dandois & Ellis, 2010, 2013;

Hugenholtz et al., 2013, 2016; Jensen & Mathews, 2016). This is because 3D reconstruction of features with SfM-MVS requires multiple images capturing the same feature, and this requirement is challenging to fulfill in environments where the RGB sensor is occluded from the feature of interest. In natural settings, vegetation may cause substantial occlusion of the ground surface, resulting in low feature matching across images and poor topographical reconstruction.

Furthermore, ground surface elevation errors may propagate aboveground measurement errors, with particular implications for applications relying on accurate measurements of vegetation height. In addition to occlusion, vegetation may pose other significant challenges to UAV-SfM: (i) wind-blown vegetation, like any non-static feature, could also create difficulties in feature matching, and (ii) vegetation's complex structure may be difficult to reconstruct (Lisein et al., 2013; Carrivick et al., 2016). Previous studies testing the vegetation height accuracy of UAV-SfM data have focused on measuring tree heights. Dandois and Ellis (2010) calculated the tree height accuracy of UAV-SfM using trees ranging in height from 4.30 m to 33.60 m, and obtained root mean square errors (RMSEs) of 3.28 m to 3.76 m. Zarco-Tejada et al. (2014) calculated UAV-SfM tree height accuracy in an olive orchard containing 152 olive trees distributed in rows with heights ranging from 1.16 m to 4.38 m, and obtained a tree height RMSE of 0.35 m. Wallace et al. (2016) calculated the tree height accuracy of UAV-SfM using 112 single-species tree with heights ranging from 4.7 m to 16.2 m, and obtained a tree height RMSE of 1.30 m.

These previous accuracy assessments of UAV-SfM in vegetated terrain were performed in a limited variety of vegetation. However, UAV-SfM may experience variable occlusion of the ground surface with varying vegetation type, structure, density, etc. As well, different vegetation types may be more or less difficult for UAV-SfM to reconstruct. It is therefore important to explore error differences between vegetation types. Further, there is a lack of consistency in the methods used in previous studies, which makes direct comparison difficult. As such, we performed a case study to assess the vertical (ground elevation) and vegetation height accuracies of a UAV-SfM dataset at a site with six major vegetation types: coniferous trees, deciduous trees, short grass, tall grass, short shrubs, and tall shrubs. For checkpoint quantity, spatial distribution, accuracy calculation, reporting, and more, we followed the 2015 ASPRS Positional Accuracy Standards for Digital Geospatial Data (ASPRS, 2015). In addition to assessing the UAV-SfM errors, we compared the errors to the UAV-LiDAR errors from Chapter 2. Based on

previous comparisons of UAV-SfM and LiDAR, we hypothesized that the UAV-LiDAR data would have higher vertical and vegetation height accuracies (Dandois & Ellis, 2010; Jensen & Mathews, 2016; Wallace et al., 2016). Overall, this chapter provides evidence to directly assess the error magnitude differences between the two technologies and allow researchers and professionals to determine which technology is best suited for their application.

3.3 Study site

The study site is located near Bragg Creek, Alberta, Canada (50°53'24"N, 114°42'26"W), and occupies approximately 250 x 400 m of very gently sloping terrain (3° mean slope) (Figure 3.1). The perimeter and area of the site are 1.25 km and 0.10 km^2, respectively. Vegetation types present consist of coniferous trees, deciduous trees, short grass (0-0.3 m height), tall grass (> 0.3 m height), short shrubs (0-1 m height), and tall shrubs (> 1 m height) (Figure 3.2). The coniferous trees are dominated by Lodgepole Pine (*Pinus contorta*) with occasional White Spruce (*Picea glauca*). The deciduous trees are dominated by Balsam Poplar (*Populus balsamifera*). Shrubs consist of Shrubby Cinquefoil (*Dasiphora fruticose*), Bog Birch (*Betula pumila*), and Sandbar Willow (*Salix exigua*). The site also contains a pipeline right of way and a reclaimed natural gas well pad. The natural gas well pad is a fenced area that contains tall grasses whose minimum heights defined the minimum height of the tall grass class and the maximum height of the short grass class. Additional tall grass patches are located outside of the fenced natural gas well pad, distributed among the short grass areas. The site is occasionally grazed by livestock, which likely explains why the grass within the fenced area is tall (i.e., protection from grazers), while the grass outside the fenced area is predominantly short and grazed. The short and tall shrub class height ranges were defined based on strong spatial clustering of the two classes – short shrubs dominated the southern half of the site and had 0-1 m heights, while the shrubs that dominated the northern half were taller than 1 m.

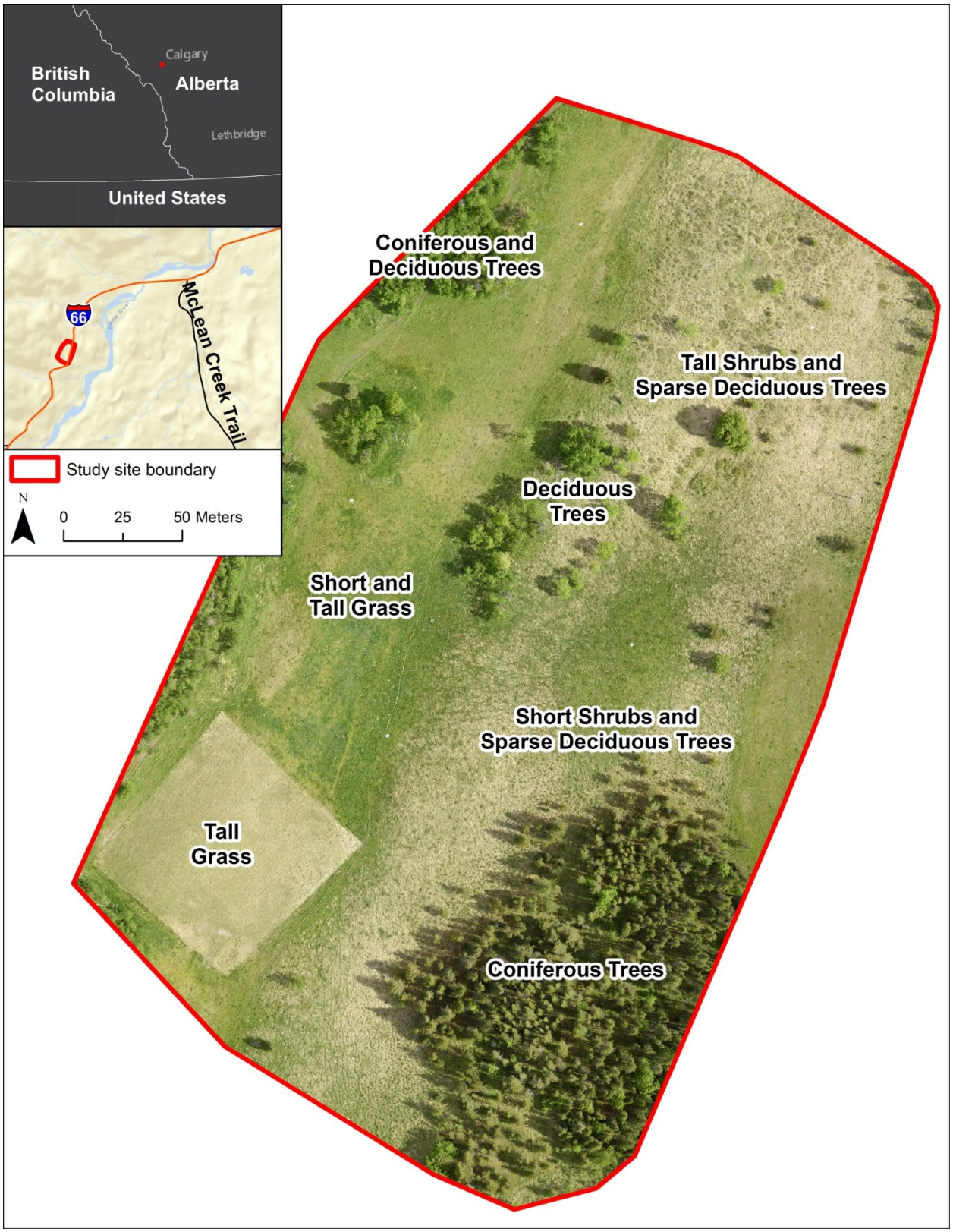

Figure 3.1 Study site location and general distribution of the six vegetation types (coniferous trees, deciduous trees, short grass, tall grass, short shrubs, and tall shrubs).

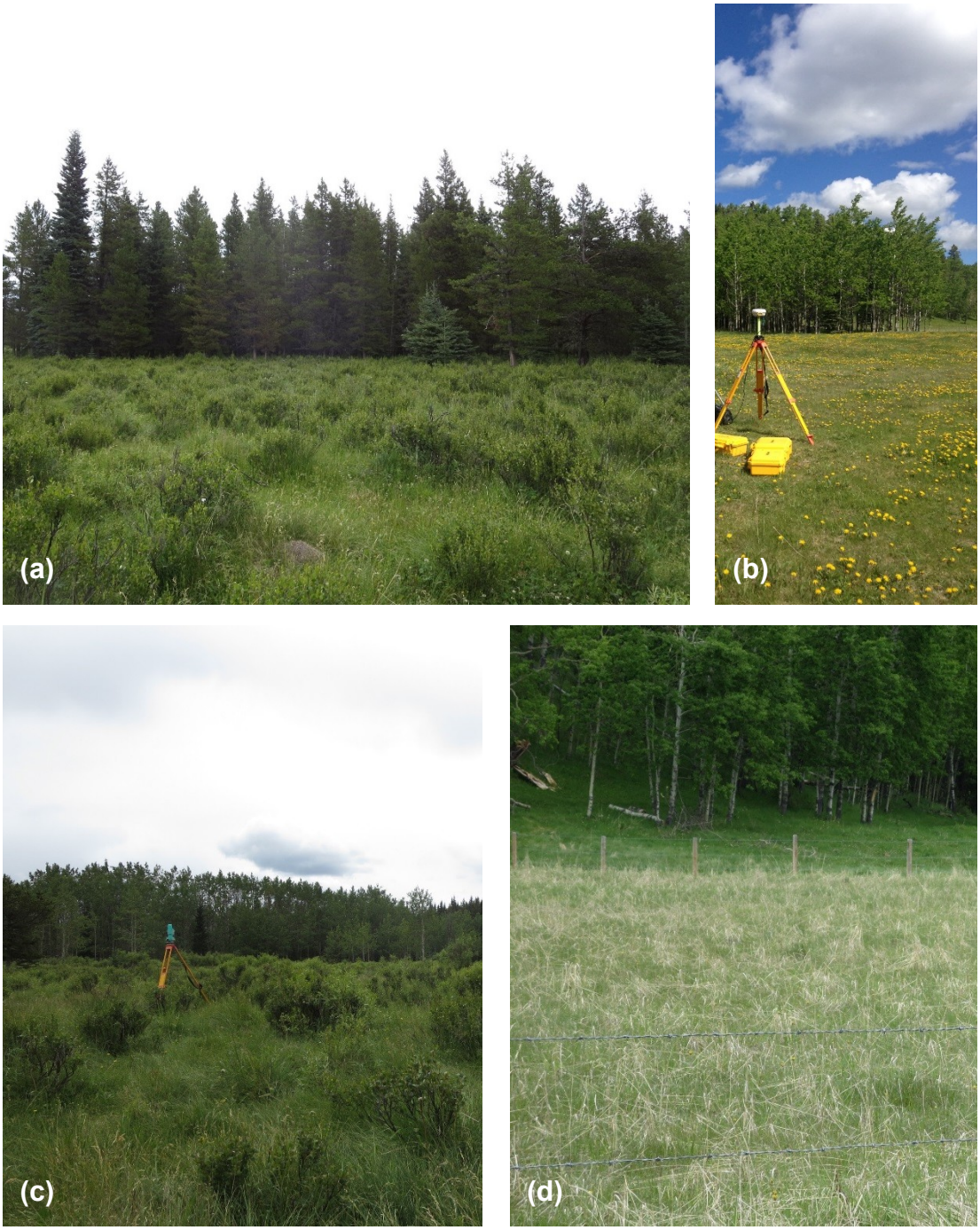

Figure 3.2 Examples of the vegetation types present throughout the study site: (a) short shrubs (foreground) and coniferous trees (background), (b) short grass (foreground) and deciduous trees (background), (c) tall shrubs (foreground) and deciduous trees (background), and (d) tall grass.

3.4 Methods

3.4.1 UAV-SfM system

The UAV-SfM system consisted of a senseFly eBee fixed-wing UAV equipped with a Canon PowerShot ELPH 110 HS 16.1 megapixel RGB camera (Figure 3.3). The eBee has a maximum take-off weight of 0.75 kg, wingspan of 0.96 m, and maximum flight time of 30-45 minutes according to site altitude, temperature, and wind. The eBee can be programmed to capture nadir (0° pitch angle) or oblique (7° or 15° pitch angle) images. Additional system specifications are summarized in Table 3.1.

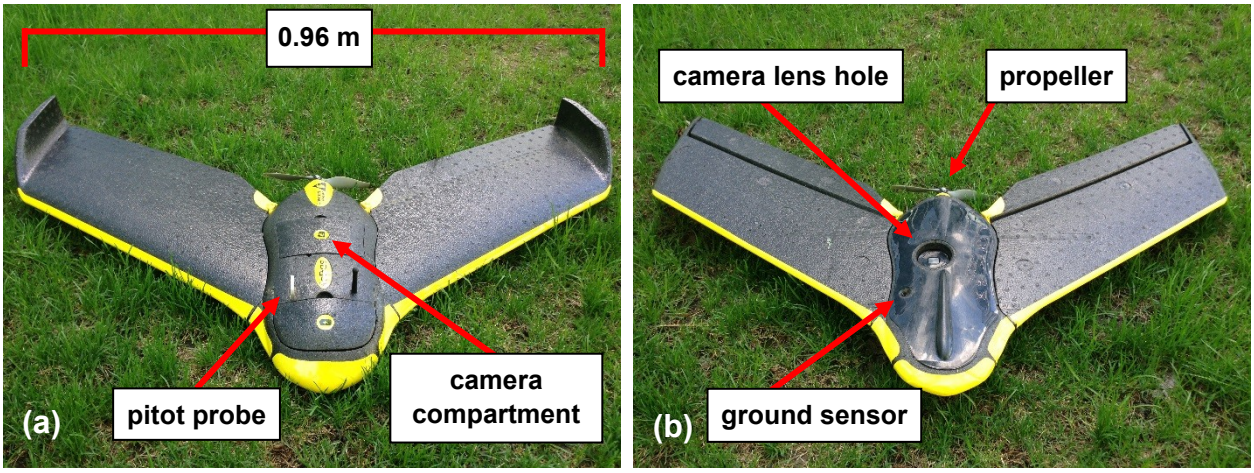

Figure 3.3 Oblique view of the UAV-SfM (a) top face and (b) bottom face .

Table 3.1 UAV-SfM system attributes.

System attribute	Properties
Wingspan	0.96 m
Maximum take-off weight	0.75 kg
Power source	3-cell lithium-polymer battery
Maximum flight time	50 min
RGB sensor	Canon PowerShot ELPH 110 HS
Optical sensor type	CMOS
Effective resolution	16.1 MP
Maximum focal length	120 mm
Maximum shutter speed	0.0005 s
Minimum aperture	f/2.7
Weight	0.135 kg

3.4.2 UAV data acquisition

The UAV-SfM flight was conducted on 02 June 2016 (the same day as the UAV-LiDAR flight in Chapter 2) during leaf-on conditions prior to the peak of the growing season, providing near-maximum leaf cover. The system flew orthogonal flight tracks to maximize multiview stereo coverage, and captured 245 oblique images (7° off nadir) with 80% longitudinal and lateral overlap from 100 m above ground level (AGL). The flight occurred at noon with overcast sky conditions in order to capture imagery with diffuse reflectance and minimal shadows. Additional flight and data properties are summarized in Table 3.2.

Table 3.2 UAV-SfM flight parameters.

Flight parameter	Properties
Flight date	02 June 2016
Flight altitude	100 m AGL
Number of flight lines and orientation	28 (orthogonal)
Images acquired	245
Image overlap	80% longitudinal, 80% lateral
Image pitch angle	7°

3.4.3 Ground control points (GCPs)

As explained in Chapter 2, a survey-grade RTK GNSS (GPS + GLONASS) was used to measure the coordinates of 7 GCPs distributed at the study site to georeference the SfM point cloud (Figure 3.4). The targets consisted of 1.2 x 1.2 m white corrugated plastic boards painted black in one quadrant, allowing the target centers to be detectable in the RGB images. The target centers were surveyed with the RTK GNSS. Special care was taken to avoid depressing the GCP center with the bottom of rover rod in order to measure the true elevation of the target center. Due to a lack of existing survey monuments near the study site, precise point positioning (PPP) was performed to establish a control point. A Trimble R4 GNSS base receiver logged raw data over a single location for approximately five hours. The base receiver data was post-processed with the Canadian Spatial Reference System (CSRS) PPP online tool to obtain a precise location of the control point. Identical to UAV data acquisition, all RTK GNSS data points were collected in the Universal Transverse Mercator (UTM) Zone 11 North (11N), North American Datum of 1983 (NAD 83) projection, with orthometric Canadian Geodetic Vertical Datum of 1928 (CGVD28) heights.

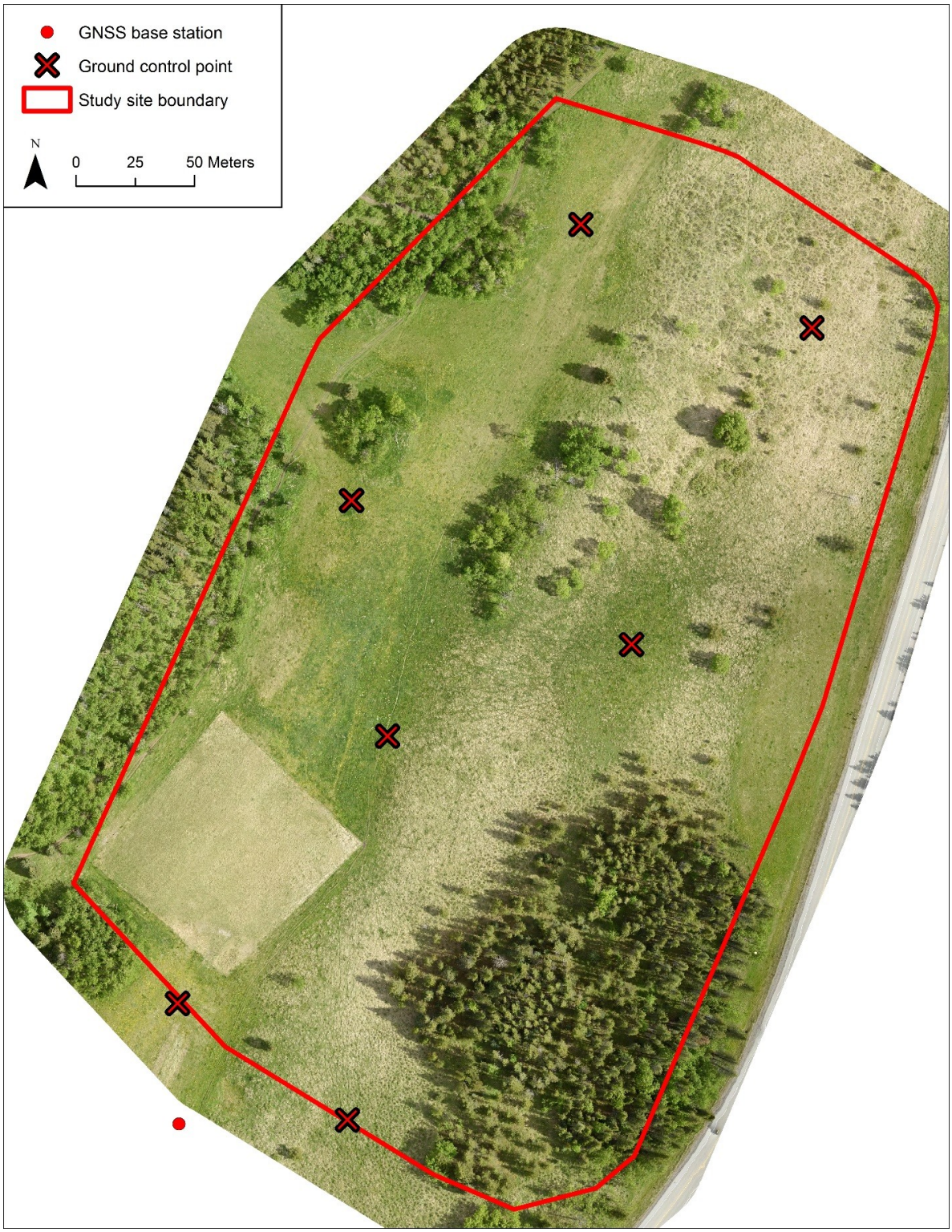

Figure 3.4 Location of RTK GNSS base station and ground control points.

3.4.4 UAV data processing

3.4.4.1 Initial processing

The RGB images were input into Pix4D SfM-MVS image processing software. SfM-MVS generally consists of the following steps. First, computer vision algorithms search through each image to identify 'features' – that is, individual pixels that are robust to changes in scale, illumination, and 3D viewing angle (Carrivick et al., 2016). Next, the features are assigned unique 'descriptors', which allow for the same features to be identified across multiple images and for the images to be approximately aligned. This initial image alignment is iteratively optimized via bundle adjustment algorithms, the output of which is a sparse 3D point cloud of feature correspondences (Westoby et al., 2012). Multiview stereo algorithms then densify the sparse point cloud, typically by two or more orders of magnitude (Westoby et al., 2012). The dense SfM point cloud was georeferenced using the 7 GCPs.

3.4.4.2 Point classification

The georeferenced and unclassified SfM point cloud was then post-processed in order to extract ground elevation and vegetation heights for the accuracy assessment. First, the point cloud was classified to separate 'ground' from 'non-ground' points. The point cloud classification method was different from Chapter 2 due to software restrictions. Accordingly, we tested three point cloud filtering methods: the Boise Center Aerospace Laboratory (BCAL) Height Filtering Tool, part of the BCAL LiDAR Tools plugin for ENVI (Streutker & Glenn, 2006), the Multiscale Curvature Classification (MCC) LiDAR command line tool (Evans & Hudak, 2007), and the Cloth Simulation Filter (CSF) available as a plugin in CloudCompare (Zhang et al., 2016). The MCC and BCAL methods were chosen for testing because they have previously been compared for LiDAR point cloud accuracy in vegetated terrain (Tinkham et al., 2011), and were developed for vegetated settings – MCC for forested and BCAL for shrub-steppe environments. The CSF method was tested because it is relatively new and supported by CloudCompare, which was built to handle large point clouds with computational efficiency.

The BCAL algorithm works by applying a minimum block filter (user-specified cell size) to the point cloud and classifying the lowest point within each grid cell as 'ground'. The ground points are then used to define a surface from a user-specified interpolation method. Unclassified points that are on or below the interpolated surface are classified as 'ground'. Then, the ground

surface is re-interpolated to include the new ground points, and additional points are classified as 'ground'. The program iterates this process until all points on or below the interpolated surface are classified as 'ground' (Streutker & Glenn, 2006).

The MCC algorithm works by first generating a raster using all of the points and a thin plate spline interpolation. The resolution of the raster is defined by the user (i.e., scale parameter, λ), and should approximately equal the average point spacing. Next, a 3 x 3 mean kernel is passed over the raster. If a point's *z*-value exceeds its corresponding raster value by more than a user-specified threshold (i.e., curvature tolerance parameter, *t*), the point is classified as 'non-ground'. The program iterates this process by generating a new mean elevation raster using the remaining unclassified points and classifying more points as 'non-ground', and terminates when it reaches a convergence threshold. The algorithm runs in three scale domains, i.e., using three resolutions for the mean elevation raster. First, the model iterates using 0.5λ and *t*, then λ and *t* + 0.1, and finally 1.5λ and *t* + 0.2 (Evans & Hudak, 2007).

One key challenge encountered with the BCAL and MCC methods was the fact that these algorithms, like most point cloud classification algorithms, were made for LiDAR point clouds, which contain smaller ground point gaps under tree canopy than SfM-derived point clouds. The size of SfM ground point gaps can often exceed optimal user-defined filter sizes (i.e., minimum block filter size for BCAL and scale parameter for MCC). If the filter is too small, it can occupy an area under canopy where only vegetation points are present – this can lead to numerous commission errors, where vegetation points are classified as 'ground' because they meet the classification criteria (i.e., a point is the lowest in the minimum block filter cell for BCAL or a point is within the curvature threshold for MCC). Setting the filter size larger to avoid such commission errors can lead to coarse ground point classification in other areas, essentially smoothing the terrain and losing potentially valuable detail.

Among the three tested filtering methods, CSF was chosen based on several factors. Like BCAL and MCC, the method only requires setting a few parameters. Second, the method can handle large point clouds efficiently – the filtering of ground points from the SfM point cloud (containing over 100 million points) took only a few seconds, compared to several hours for BCAL and MCC. There is no need to first tile or thin the point cloud, as was necessary for MCC. Third, and most importantly, the nature of the CSF algorithm results in robustness to large sub-

canopy ground point gaps inherent in SfM point clouds and therefore less commission errors than BCAL and MCC.

The CSF algorithm generally works by first inverting the point cloud and placing a simulation cloth on the surface with user-specified properties such as scene type (cloth rigidness), cloth resolution (horizontal distance between cloth nodes), and maximum number of iterations. Once the positions of the cloth nodes are optimized, the point cloud is classified. A point is classified as 'ground' if the cloud-to-cloud distance between it and the cloth nodes is within a user-specified classification threshold. After several rounds of testing, the settings that yielded the most accurate results (i.e., lowest mean absolute error using vertical checkpoints) and were thus implemented to filter the SfM point cloud were: 'Flat' for scene type, 1.5 m cloth resolution, 500 maximum iterations, and 0.10 m classification threshold. The scene type setting controls the rigidness of the simulation cloth that is placed on the surface of the inverted point cloud. The rigidness refers to the vertical mobility of cloth nodes that are over void areas of the inverted surface (i.e., areas where the inverted point cloud lacks surficial points). If a cloth node is supported by surficial points, it remains at rest. If a cloth node is unsupported, it will move downward by the force of gravity. Then, the internal forces between the node and neighboring nodes will cause upward mobility by a distance that is determined by the scene type setting – a setting of 'Flat' produces the most rigid cloth with the highest upward travel distance for these nodes, and a setting of 'Steep slope' produces the least rigid cloth with the least upward travel. Once the simulation cloth is set on the surface of the inverted point cloud, points are classified as ground if they are within a threshold distance to the cloth (i.e., classification threshold). The CSF developers note that, in areas of the point cloud where the terrain slope deviates from the scene type setting, the increased distance between the cloth and the inverted point cloud may cause points to be misclassified as non-ground (Zhang et al., 2016). To help alleviate misclassification errors associated with heterogeneous terrain slope, the CSF tool has a slope post-processing feature that can be enabled before the algorithm is run in order to fit the simulation cloth more closely to the inverted point cloud's surface, although it was not used in this study.

3.4.4.3 Rasterization

Following point classification, the ground-classified points were used to construct a DTM. To compute the DTM, the ground points were interpolated with minimum binning – each cell was assigned the minimum elevation value of the points found within its extent. Natural neighbor interpolation was then used to compute the elevation values of cells without points. This DTM interpolation method was chosen based on testing several other methods including: (i) minimum binning with linear interpolation for empty cells, (ii) inverse distance weighted (IDW) binning with linear (and natural neighbor) interpolation for empty cells, (iii) average binning with linear (and natural neighbor) interpolation for empty cells, (iv) nearest neighbor binning with linear (and natural neighbor) interpolation for empty cells, and (v) triangulated irregular network (TIN) with the ground-classified points and interpolating using linear (and natural neighbor). Of these methods, minimum binning with natural neighbor interpolation for empty cells produced the lowest mean absolute error using vertical checkpoints. The chosen DTM resolution was 0.30 m because it yielded a lower mean absolute error using vertical checkpoints than the other tested DTM resolutions, which ranged from 0.05 m (because the average ground point spacing of the SfM point cloud was 0.05 m) to 0.30 m with every 0.05 m increment tested.

To eventually extract tree, grass, and shrub heights from the SfM data, we used the same procedure that was used for the UAV-LiDAR data in Chapter 2. We computed a digital canopy height model (DCHM) from the SfM data using the following steps. First, all of the points (ground and non-ground) were interpolated into a 0.30 m digital surface model (DSM) using maximum binning with natural neighbor interpolation for empty cells. The 0.30 m DCHM was computed by subtracting the DTM from the DSM. This workflow is generally consistent with previous studies, with variations in interpolation methods (Persson et al., 2002; Gaveau & Hill, 2003; Zimble et al., 2003; Clark et al., 2004; Hirata, 2004; Maltamo et al. 2004; Suarez et al., 2005; Kwak et al., 2007; Glenn et al., 2011). Another DSM interpolation method was tested by first thinning the points with a 0.30 m maximum grid, then constructing a TIN and using natural neighbor interpolation to create a 0.30 m DSM. However, maximum binning with natural neighbor interpolation produced a DSM and DCHM with the lowest combination of mean absolute errors in each vegetation type using vegetation height checkpoints. Other DSM resolutions were tested as well, from 0.05 m (because the average point spacing of the SfM point cloud was 0.04 m) to 0.50 m, with every 0.05 m increment tested. The 0.30 m DSM produced the

DCHM with the lowest combination of mean absolute errors in each vegetation type using vegetation height checkpoints.

3.4.5 Reference data acquisition

The UAV-SfM data were collected on 02 June 2016. Field-based reference measurements of shrub and grass height were collected on 14-16 June 2016, and tree heights were measured on 22 June to 07 July 2016. Ground surface elevation reference measurements were collected on 05-21 August 2016.

3.4.5.1 Ground surface elevation

Ground surface elevation reference measurements were collected at random locations throughout the study site, and were compared to the interpolated ground elevation values of the DTM. In areas of little to no canopy cover, an RTK GNSS survey was performed to measure elevation at 731 vertical checkpoints. A SECO topo shoe with a wide, flat, circular base was attached to the bottom of the RTK rover rod to avoid depressing the rod into the ground and under-measuring elevation. Within the coniferous tree areas, where canopy cover prohibited adequate satellite geometry for RTK GNSS collection, a Nikon DTM-522 Total Station was used to obtain 131 random elevation measurements. In total, 862 vertical checkpoints were collected during the RTK and Total Station surveys. The measurements were randomly distributed among the vegetation types in a stratified manner, with 103 coniferous tree, 50 deciduous tree, 222 short grass, 105 tall grass, 305 short shrub, and 77 tall shrub vertical reference measurements.

3.4.5.2 Vegetation height

We used the same vegetation height checkpoints that were used to assess the accuracy of the UAV-LiDAR data in Chapter 2. A Total Station was used to measure tree heights using the following steps. First, the Total Station was set up over a control point established with the RTK GNSS. A reflective prism was positioned by an assistant against the tree and its height was manually adjusted until its center was aligned horizontally to the height mark on the Total Station. The Total Station operator acquired a laser distance measurement to the prism, while the assistant recorded the height of the prism above ground level with a steel tape measure. The

angle of the Total Station when the telescope was aimed at the tree top was then recorded. In total, 74 coniferous and 48 deciduous tree heights were measured using this method.

Height measurements of grasses and shrubs were acquired with a steel tape measure, while the coordinates of each measurement were recorded by the RTK GNSS. For grasses, a 0.5 m diameter ring was randomly placed on the surface. The RTK rover rod was placed inside the ring, near the point of maximum plant height, and the distance from the ground surface to the top of the plant was measured. For shrubs, the RTK rover rod was placed next to the shrub and the distance from the ground surface to the top of the plant was measured. In total, 49 short grass patches, 75 tall grass patches, 84 short shrubs, and 63 tall shrubs were measured in the field.

3.4.6 Data analysis

3.4.6.1 Ground elevation accuracy

Ground elevations were extracted from the DTM at each of the 862 vertical checkpoint locations. The 862 reference elevation measurements (z_{ref}) collected with the RTK GNSS and Total Station were compared against their respective DTM values (z_{DTM}) and residuals were calculated ($z_{\text{DTM}} - z_{\text{ref}}$). According to ASPRS (2015) recommendations, the frequency distributions of residuals overall and per vegetation type were considered in order to choose the appropriate statistic for vertical accuracy. Due to non-normal distributions of residuals, vertical error was calculated as the 95$^{\text{th}}$ percentile absolute error (Q_{95}):

$$Q_{95} = \left(A[n_w] + \left(n_d * (A[n_w + 1] - A[n_w])\right)\right) \quad \text{[Eq.1]}$$

where A is an array of the absolute values of the samples, indexed in ascending order from *1* to *N*, *A[i]* is the sample value of array A at index *i* (e.g., n_w or n_d), *i* is an integer between *1* and *N*, *n* is the rank of the observation that contains the 95$^{\text{th}}$ percentile, n_w is the whole number component of *n*, and n_d is the decimal component of *n* (ASPRS, 2015).

3.4.6.2 Vegetation height accuracy

Grass and shrub heights were extracted from the DCHM using the sample locations from the field measurements. The coordinates of trees from the Total Station measurements were used to make 1 m tree buffers. The maximum DCHM value within each 1 m tree buffer was extracted. In

total, 74 coniferous trees, 48 deciduous trees, 49 short grasses, 75 tall grasses, 84 short shrubs, and 63 tall shrubs were analyzed. The field-derived reference height measurements (h_{ref}) were compared against the respective DCHM values (h_{DCHM}) and residuals were calculated ($h_{DCHM} - h_{ref}$). Due to non-normal distributions of residuals, vegetation height error was calculated as the 95th percentile absolute error.

3.5 Results and discussion

3.5.1 Point cloud properties

The classified SfM point cloud was clipped to the 0.10 km^2 site boundary and point cloud properties were extracted (Table 3.3). The point cloud contained 60,569,479 total points, approximately 62% of which the CSF algorithm classified as ground. Average ground point density and spacing were 417 pts/m^2 and 0.05 m, respectively. Figure 3.5 shows the spatial distribution of the ground point coverage and density. Ground point gaps accounted for 10% of the study site area. There are large ground point gaps in the coniferous tree area in the southern end of the site, encompassing approximately 42% of the coniferous tree area, with other large gaps occurring along the northwestern edge and interior of the study site, mostly where deciduous trees are located. These ground point gaps demonstrate that due to occlusions from tree canopy, UAV-SfM was unable to consistently resolve the ground surface.

Table 3.3 UAV-SfM point cloud attributes (clipped to 0.10 km^2 site boundary).

Point cloud attribute	Properties
Total points	60,569,479
Average point density	595 pts/m^2
Average point spacing	0.04 m
Ground-classified points (% of total)	37,422,106 (62%)
Average ground point density	417 pts/m^2
Average ground point spacing	0.05 m
Average non-ground point density	297 pts/m^2
Average non-ground point spacing	0.06 m
Horizontal coordinate system and datum	UTM Zone 11N NAD 83
Vertical datum	CGVD28

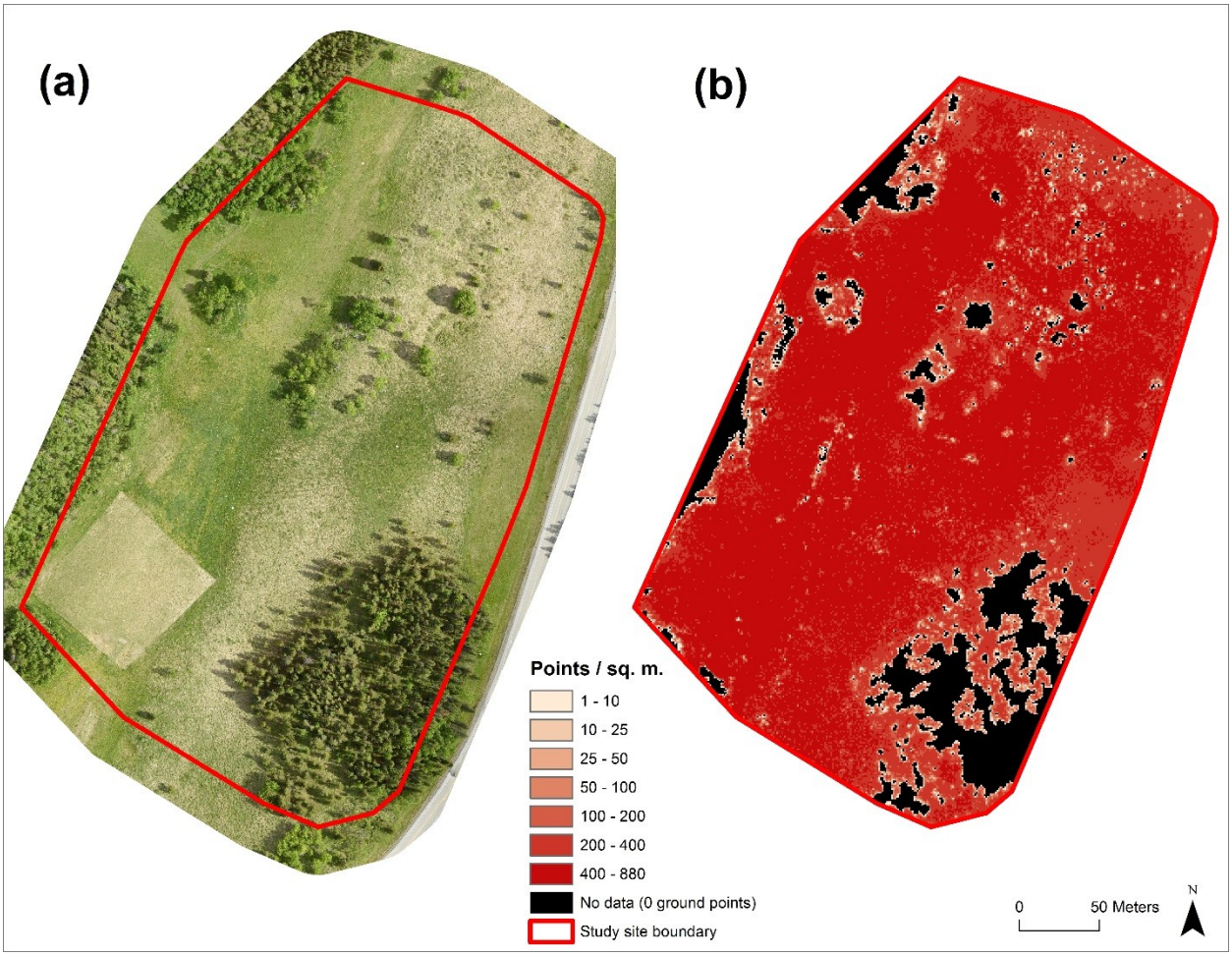

Figure 3.5 (a) Study site boundary and orthomosaic image and (b) ground-classified point density (pts/m^2) of UAV-SfM point cloud. Data gaps (no ground classified points) are shown in black.

3.5.2 Ground surface elevation errors

To calculate vertical errors of the SfM data, the ground surface elevations at the 862 random vertical checkpoint locations were extracted from the DTM and compared against field measured elevations, and residuals ($z_{DTM} - z_{ref}$) were calculated overall and for each vegetation type (Table 3.4). The residuals ranged from -0.20 m for coniferous and deciduous trees to 0.35 m for short shrubs. Figure 3.6b shows the spatial distribution of absolute vertical error. Some of the highest absolute vertical errors occurred within the ground point gaps. The lowest median error occurred in coniferous trees, which was unexpected given the large ground point gaps within the coniferous tree area. Many vertical checkpoints were located within these ground point gaps, so field reference measurements were compared against interpolations made across large areas. The resultant absolute vertical errors ranged from 0.01 m to 0.25 m.

Table 3.4 UAV-SfM vertical error statistics. The One-Sample Sign test (α level of 0.05) contained a null hypothesis that the median residual equals 0.00 m, and an alternative hypothesis that the median residual is greater than 0.00 m – bold *p*-values indicate the median residual is significantly greater than 0.00 m.

Vegetation type	*n*	Median error (interquartile range) (m)	*p*-value (95% confidence interval) of One-Sample Sign test	Min. error, max. error (m)	95th percentile absolute error (m)
All (combined)	862	0.05 (0.08)	**0.0000** (0.0499, 0.0590)	-0.20, 0.35	0.17
Coniferous trees	103	0.01 (0.11)	0.3467 (-0.0119, 0.0201)	-0.20, 0.25	0.20
Deciduous trees	50	0.04 (0.11)	**0.0013** (0.0300, 0.0607)	-0.20, 0.20	0.20
Short grass	222	0.05 (0.06)	**0.0000** (0.0430, 0.0590)	-0.07, 0.21	0.14
Tall grass	105	0.11 (0.10)	**0.0000** (0.0849, 0.1243)	-0.10, 0.25	0.21
Short shrubs	305	0.05 (0.06)	**0.0000** (0.0440, 0.0550)	-0.16, 0.35	0.16
Tall shrubs	77	0.08 (0.07)	**0.0000** (0.0634, 0.0967)	-0.06, 0.33	0.26

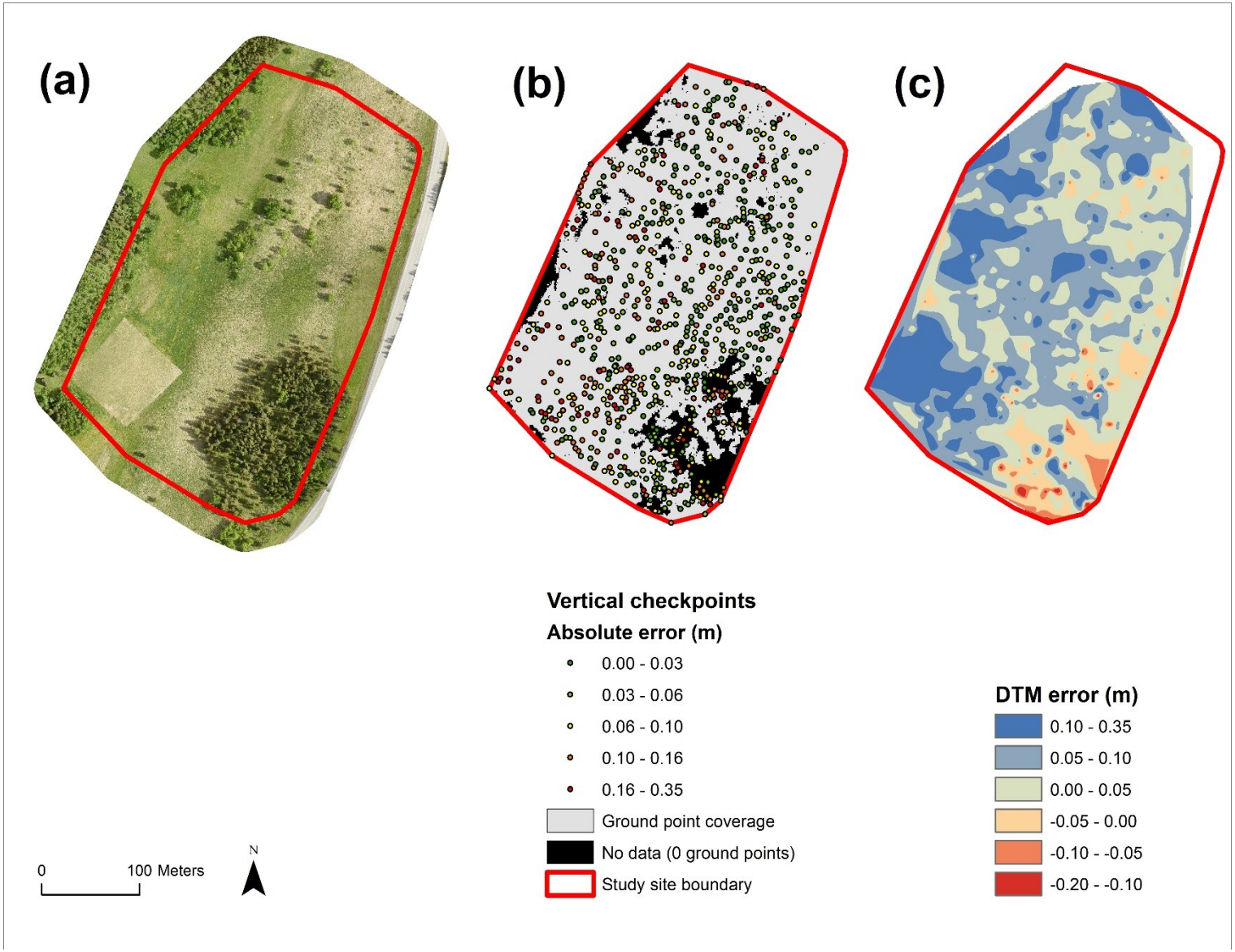

Figure 3.6 (a) Study site orthomosaic image, (b) UAV-SfM vertical checkpoints colored by absolute vertical error, and (c) DTM error raster interpolated with the vertical checkpoint errors.

Since most of the median errors were positive, a One-Sample Sign test (α level of 0.05) was performed for all the data combined and for each vegetation type to determine if the median residual was significantly greater than 0.00 m. This test was used to determine if the SfM data had a tendency to overestimate ground elevation. The *p*-values from the One-Sample Sign test (Table 3.4) indicate that SfM tended to overestimate ground elevation in all vegetation types except coniferous trees. This is visually illustrated in Figure 3.6c, which shows a DTM error raster interpolated using the vertical error at each vertical checkpoint. Most of the raster errors are positive, and negative errors mainly occur in the coniferous tree area. These negative errors can be explained by the median error in coniferous trees, which is the lowest median error (i.e., 0.01 m), and the ground point gaps that account for 42% of the coniferous tree area. The interpolation of errors across the large ground point gaps caused negative values in the coniferous tree area of the raster. In general, SfM had a tendency to overestimate ground elevation, and this suggests that overall, the ground surface was not resolved in the SfM dataset, such that the lowest points classified as ground in the SfM point cloud were vegetation. These commission errors resulted in most median vertical errors significantly greater than 0.00 m.

The median residuals of each vegetation type were compared to those of other vegetation types in order to determine if they significantly differ. First, a Shapiro-Wilk test (α level of 0.05) and a visual inspection of the histograms, normal Q-Q plots, and box plots indicated that not all vegetation types had normal distributions of residuals (Figure 3.7). Due to the non-normality of residuals in some vegetation types, a non-parametric Levene's test (α level of 0.05) was used to inspect equality of variance among the residuals in each vegetation type pair in order to determine which median-comparison hypothesis test to perform. The *p*-values from the non-parametric Levene's test indicated inequality of variance (heteroscedasticity) among the residuals of several vegetation type pairs. Due to the non-normality and heteroscedasticity, a Mood's Median test (α level of 0.05) was performed on vegetation type pairs in order to determine if median residuals between vegetation type pairs were significantly different. The *p*-values from the Mood's Median test (Table 3.5) indicated significant differences in median residuals between all vegetation type pairs except: deciduous trees and short grass, deciduous trees and short shrubs, and short grass and short shrubs.

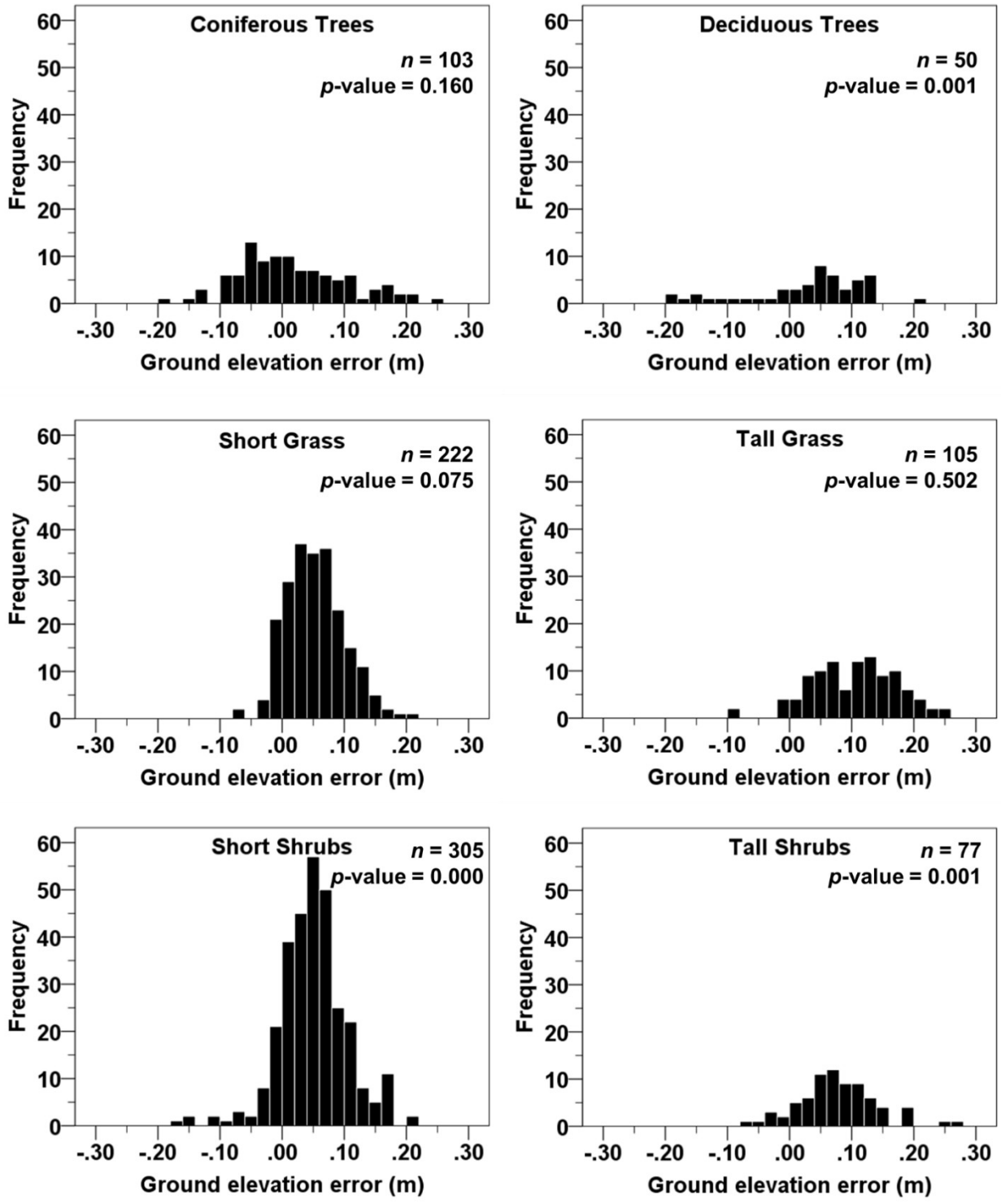

Figure 3.7 Histograms of UAV-SfM vertical error and *p*-values from a Shapiro-Wilk normality test (α level of 0.05) for each vegetation type.

Table 3.5 *p*-values and 95% confidence intervals of Mood's Median test (α level of 0.05) performed on the UAV-SfM median vertical residuals of vegetation type pairs. The Mood's Median test contained a null hypothesis that median residuals of the two vegetation types are equal, and an alternative hypothesis that there is a difference between the median residuals – bold *p*-values indicate the median vertical residuals significantly differ between the two vegetation types.

Vegetation type	Coniferous trees	Deciduous trees	Short grass	Tall grass	Short shrubs
Deciduous trees	**0.005** (-0.070,-0.023)				
Short grass	**0.001** (-0.065,-0.024)	0.531 (-0.0230,0.014)			
Tall grass	**0.000** (-0.131,-0.073)	**0.001** (-0.087,-0.040)	**0.000** (-0.078,-0.031)		
Short shrubs	**0.001** (-0.063,-0.026)	0.371 (-0.021,0.012)	0.752 (-0.010,0.012)	**0.000** (-0.077,-0.033)	
Tall shrubs	**0.000** (-0.100,-0.045)	**0.005** (-0.052,-0.011)	**0.005** (-0.047,-0.011)	**0.024** (0.003,0.056)	**0.001** (-0.047,-0.011)

Due to the non-normality of residuals (Figure 3.7), vertical accuracy was calculated as the 95th percentile absolute error (Q_{95}) overall and per vegetation type (Table 3.4), as recommended by ASPRS (2015). The Q_{95} values ranged from 0.14 m for short grass to 0.26 m for tall shrubs. The lowest Q_{95} occurring in short grass likely reflects the fact that this was the shortest vegetation type (0.0 m to 0.3 m height) in the study area, which should minimize vertical errors of the ground surface elevation. The largest Q_{95} occurred in tall shrubs; the five largest vertical errors for SfM occurred in short and tall shrubs, where the ground elevation was overestimated by 0.25-0.35 m. The overall vertical Q_{95} value was 0.17 m; therefore, the UAV-SfM data meet the requirements of a 0.17 m vertical accuracy class, and have a 0.51 m vegetated vertical accuracy (VVA) at the 95% confidence level (ASPRS, 2015).

3.5.3 Vegetation height errors

Vegetation heights measured in the field ranged from: (i) coniferous trees (3.79 m to 23.24 m), (ii) deciduous trees (8.18 m to 17.33 m), (iii) short grass (0.03 m to 0.30 m), (iv) tall grass (0.31 m to 1.13 m), (v) short shrubs (0.40 m to 0.99 m), and (vi) tall shrubs (1.03 m to 1.83 m). The vegetation heights at the 393 checkpoints were extracted from the DCHM and compared against field measured heights, and residuals ($h_{\mathrm{DCHM}} - h_{\mathrm{ref}}$) were calculated overall and for each vegetation type (Table 3.6). A Shapiro-Wilk test (α level of 0.05) and a visual inspection of the histograms, normal Q-Q plots, and box plots indicated that not all vegetation types had normal distributions of residuals (Figure 3.8). Therefore, non-parametric statistical tests were performed on the residuals. The residuals ranged from -8.45 m for coniferous trees to 4.89 m for tall shrubs. Median errors ranged from -0.10 m for short grass to -0.54 m for deciduous trees. The lowest absolute median error was expected, as short grass is the shortest vegetation type (0.0 m to 0.3 m height).

Since all of the median errors were negative, a One-Sample Sign test (α level of 0.05) was performed on the residuals. This test was used to determine if the SfM data had a tendency to underestimate vegetation height. The *p*-values from the One-Sample Sign test (Table 3.6) indicate that the median errors are significantly less than 0.00 m overall and for every vegetation type. The tendency of SfM to underestimate vegetation height is likely due to one or both of the following: (i) overestimating ground elevation and (ii) not capturing the highest point at each vegetation height checkpoint.

Table 3.6 UAV-SfM vegetation height error statistics. The One-Sample Sign test (α level of 0.05) contained a null hypothesis that the median residual equals 0.00 m, and an alternative hypothesis that the median residual is less than 0.00 m – bold p-values indicate the median residual is significantly less than 0.00 m.

Vegetation type	*n*	Median error (interquartile range) (m)	*p*-value (95% confidence interval) of One-Sample Sign test	Min. error, max. error (m)	95th percentile absolute error (m)
All (combined)	393	-0.34 (0.35)	**0.0000** (-0.3780, -0.3076)	-8.45, 4.89	1.35
Coniferous trees	74	-0.30 (0.54)	**0.0000** (-0.4237, -0.2418)	-8.45, 3.92	2.58
Deciduous trees	48	-0.54 (0.83)	**0.0000** (-0.7052, -0.3152)	-4.97, 0.95	2.29
Short grass	49	-0.10 (0.11)	**0.0000** (-0.1428, -0.1017)	-0.35, 0.09	0.22
Tall grass	75	-0.30 (0.14)	**0.0000** (-0.3669, -0.2933)	-0.88, 0.91	0.67
Short shrubs	84	-0.43 (0.22)	**0.0000** (-0.4761, -0.3991)	-0.83, -0.07	0.70
Tall shrubs	63	-0.50 (0.61)	**0.0000** (-0.6675, -0.4060)	-1.54, 4.89	1.36

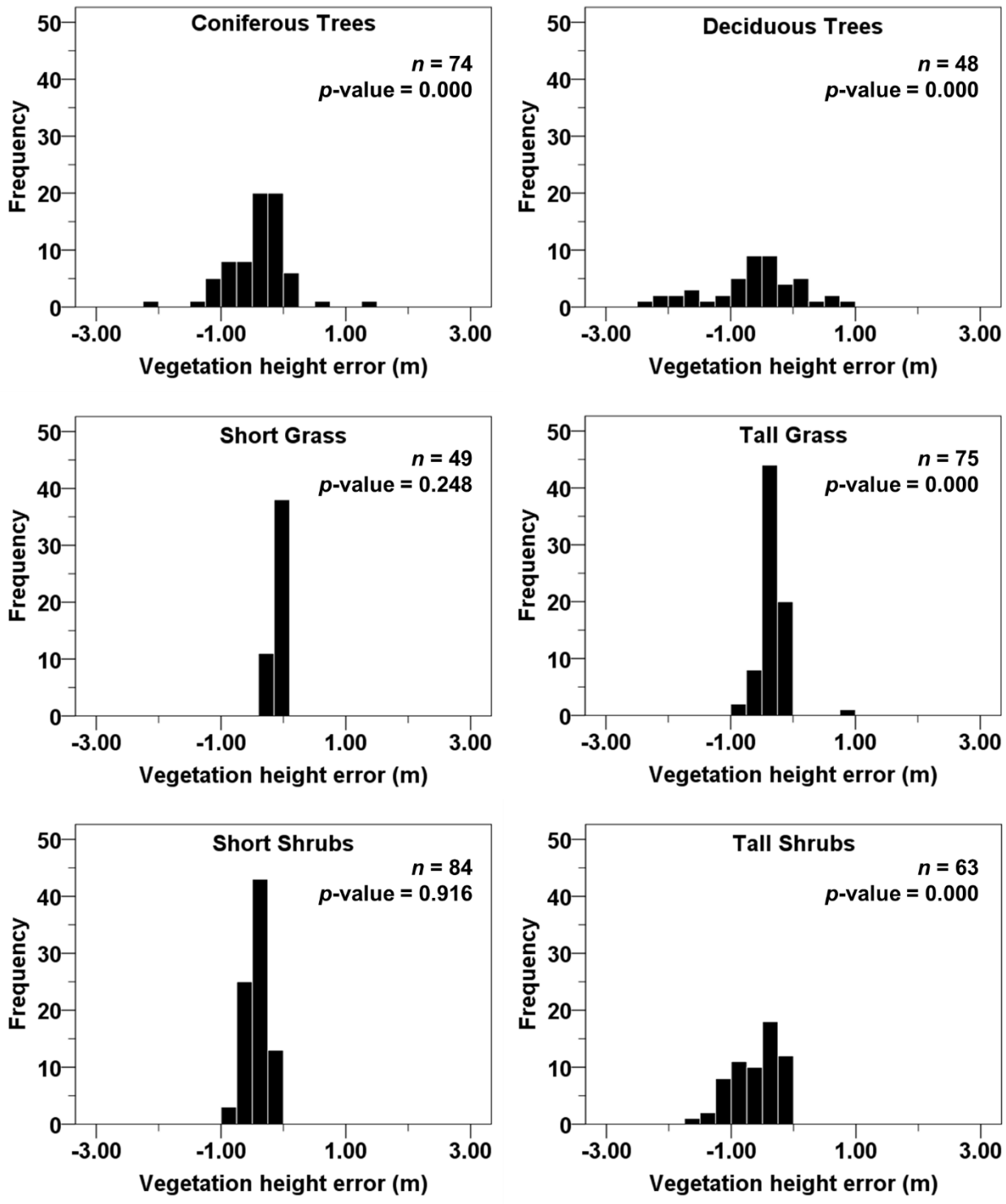

Figure 3.8 Histograms of UAV-SfM vegetation height error and *p*-values from a Shapiro-Wilk normality test (α level of 0.05) for each vegetation type.

The median residuals of each vegetation type were compared to those of the other vegetation types in order to determine if they differed significantly. First, due to the non-normality of residuals in some vegetation types (Figure 3.8), a non-parametric Levene's test (α level of 0.05) was used to inspect equality of variance among the residuals in each vegetation type pair in order to determine which median-comparison hypothesis test to perform. The *p*-values from the non-parametric Levene's test indicated inequality of variance (heteroscedasticity) among the residuals of several vegetation type pairs. Due to the non-normality and heteroscedasticity, a Mood's Median test (α level of 0.05) was performed on vegetation type pairs in order to determine if median residuals between vegetation type pairs were significantly different. The *p*-values from the Mood's Median test (Table 3.7) indicated significant differences in median residuals between all but five vegetation type pairs: coniferous trees and deciduous trees, coniferous trees and tall grass, deciduous trees and short shrubs, deciduous trees and tall shrubs, and short shrubs and tall shrubs. The highest *p*-values occurred for the following pairs: (i) coniferous trees and tall grass, 0.935, (ii) deciduous trees and short shrubs, 0.469, and (iii) deciduous trees and tall shrubs, 0.764. For all these pairs, these high *p*-values can be explained by the similar median errors and large interquartile ranges.

Due to the non-normality of the residuals (Figure 3.8), vegetation height accuracy was calculated as the 95th percentile absolute error (Q_{95}) overall and per vegetation type (Table 3.6). The Q_{95} values ranged from 0.22 m for short grass to 2.58 m for coniferous trees. The lowest Q_{95} occurred in short grass, which likely reflects the fact that short grass is the shortest vegetation type (0.0 m to 0.3 m height). The largest Q_{95} occurred in coniferous trees, which could be a result of the ground point gaps accounting for 42% of the coniferous tree area. The overall vegetation height Q_{95} value was 1.35 m, however, the large range (i.e., 2.36 m) among the vegetation types demonstrates the importance of considering vegetation type-specific errors.

Table 3.7 *p*-values and 95% confidence intervals of Mood's Median test (α level of 0.05) performed on the UAV-SfM median vegetation height residuals of vegetation type pairs. The Mood's Median test contained a null hypothesis that median residuals of the two vegetation types are equal, and an alternative hypothesis that there is a difference between the median residuals – bold *p*-values indicate the median vertical residuals significantly differ between the two vegetation types.

Vegetation type	Coniferous trees	Deciduous trees	Short grass	Tall grass	Short shrubs
Deciduous trees	0.138 (-0.077,0.364)				
Short grass	**0.000** (-0.319,-0.163)	**0.000** (-0.534,-0.246)			
Tall grass	0.935 (-0.132,0.049)	**0.012** (-0.366,-0.009)	**0.000** (0.161,0.232)		
Short shrubs	**0.026** (0.000,0.207)	0.469 (-0.229,0.138)	**0.000** (0.298,0.380)	**0.000** (-0.195,-0.089)	
Tall shrubs	**0.013** (0.043,0.362)	0.764 (-0.182,0.270)	**0.000** (0.346,0.511)	**0.000** (0.130,0.361)	0.273 (-0.018,0.225)

3.5.4 Comparison to UAV-LiDAR

Before comparing the UAV-SfM ground elevation and vegetation height errors to those obtained by the UAV-LiDAR dataset in Chapter 2, it is important to address the similarities and differences between the two analyses. The UAV-LiDAR and UAV-SfM datasets were both acquired on the same day, over the same study area, and used the same ground control points for georeferencing. Both analyses used the same vegetation height ground reference measurements. For the vegetation height accuracy analysis of both datasets, an identical processing workflow was used to produce a DCHM and to extract vegetation heights from the DCHM. However, the two analyses used different ground surface elevation reference measurements; the UAV-LiDAR analysis used 445 vertical checkpoints that were co-located with LiDAR points, so vertical errors were calculated using the point elevation values (i.e., using a point-to-point method). The UAV-SfM analysis used 862 randomly distributed ground surface elevation reference measurements, and vertical errors were calculated using a DTM (i.e., a point-to-surface method). Additionally, the UAV-SfM point cloud was classified using a different ground point filtering algorithm than the one used for the UAV-LiDAR point cloud in Chapter 2. In summary, there are limitations to the comparison between the UAV-SfM and UAV-LiDAR datasets that include different point classification algorithms and the ground surface reference measurements.

3.5.4.1 Ground elevation errors

In terms of ground surface elevation errors, SfM median errors among the vegetation types ranged from 0.01 m for coniferous trees to 0.11 m for tall grass, and LiDAR median errors ranged from 0.00 m for coniferous trees and short grass to 0.04 m for short shrubs. LiDAR had a lower median error overall and in every vegetation type. SfM median errors were significantly above 0.00 m in every vegetation type except coniferous trees, and LiDAR median errors were significantly above 0.00 m in every vegetation type except coniferous trees and short grass, where the median errors were 0.00 m. SfM had a larger range (i.e., 0.55 m) of minimum and maximum error than LiDAR (i.e., 0.22 m).

The 95th percentile absolute errors (Q_{95}) for SfM ranged from 0.14 m for short grass to 0.26 m for tall shrubs. For LiDAR, Q_{95} ranged from 0.06 m for short grass to 0.11 m for deciduous trees. The lowest Q_{95} for SfM and LiDAR occurred in short grass, which likely

reflects the fact that short grass is the shortest vegetation type (0.0 m to 0.3 m height). SfM had the largest Q_{95} in tall shrubs and tall grass (i.e., 0.26 m and 0.21 m, respectively), where likely the density of the tall vegetation substantially occluded the ground surface more than the other vegetation types. Thus, the lowest points that were reconstructed by SfM pertained to vegetation, but were likely misclassified as ground points, resulting in high errors. LiDAR had the largest Q_{95} in deciduous trees, short shrubs, and tall shrubs (i.e., 0.11 m, 0.09 m, and 0.09 m, respectively). As previously mentioned in Chapter 2, the ground cover underneath deciduous trees included short shrubs and tall shrubs, which can help explain the similar Q_{95} values. The laser pulse was able to similarly penetrate the short and tall shrubs given the similar structure and foliage density of the shrubs.

In summary, UAV-LiDAR outperformed UAV-SfM in ground elevation measurement accuracy overall and in every vegetation type. UAV-SfM had a higher tendency to overestimate ground elevation, as demonstrated by more vegetation type-specific median errors significantly above 0.00 m than UAV-LiDAR, and the higher median errors in every vegetation type than UAV-LiDAR. UAV-SfM had the lowest ground elevation accuracy in tall shrubs and tall grass, and UAV-LiDAR had the lowest ground elevation accuracy in deciduous trees, short shrubs, and tall shrubs.

3.5.4.2 Vegetation height errors

In terms of vegetation height errors, the SfM residuals ranged from -8.45 m for coniferous trees to 4.89 m for tall shrubs, while the LiDAR residuals ranged from –13.38 m for coniferous trees to 5.97 m for short shrubs. Figure 3.9 shows the spatial distribution of absolute vegetation height error for (a) SfM and (b) LiDAR. The two highest vegetation height errors for SfM are marked as (c) and (d), and the two highest errors for LiDAR are marked as (e) and (f). Interestingly, at each of the four checkpoints, the SfM and LiDAR errors differed by 3.17 m to 13.16 m. To investigate the differences of vegetation height in the SfM and LiDAR datasets at these checkpoints, we extracted profiles from the point cloud at each checkpoint, as shown in Figure 3.9. In Figures 3.9c and 3.9d it can be seen that the coniferous and deciduous trees are not fully reconstructed by SfM. These two trees are relatively isolated (i.e., there are few to no adjacent trees), therefore, the RGB imagery should have captured multiple viewpoints of the tree for

proper reconstruction. In Figures 3.9e and 3.9f it can be seen that the LiDAR error is much higher for the coniferous trees located on the edge of the LiDAR data, where all the points were acquired at high scan angles (i.e., 30-40°) and the maximum scan angle of 40° could not capture the tops of trees. These errors are expected and preventable (e.g., capture an extra flight line of LiDAR data over trees on the edge of the site plot, and fly higher), whereas the two highest SfM errors were unexpected, especially considering the isolation of the trees that weren't fully reconstructed.

SfM median errors ranged from -0.10 m for short grass to -0.54 m for deciduous trees. LiDAR median errors ranged from -0.20 m for short grass to -0.48 m for deciduous trees. The lowest absolute median errors for both datasets are expected, as short grass is the shortest vegetation type (0.0 m to 0.3 m height). For both datasets, the median error of every vegetation type was significantly below 0.00 m, indicating both datasets had a tendency to underestimate vegetation height.

The 95th percentile absolute errors (Q_{95}) were calculated in order to estimate SfM and LiDAR vegetation height accuracy overall and per vegetation type. In terms of Q_{95}, LiDAR had a higher vegetation height accuracy overall and for deciduous trees, short shrubs, and tall shrubs. The lower vegetation height accuracy of SfM in these vegetation types can be explained by: (i) the complex structure of shrubs and deciduous tree crowns, which may be difficult for SfM to reconstruct, and (ii) the lower ground elevation accuracy of SfM relative to LiDAR in these vegetation types. Conversely, the higher vegetation height accuracy of SfM in short grass and tall grass, despite its lower ground elevation accuracy relative to LiDAR, could be due to the much higher average point density (i.e., 595 pts/m^2 for SfM versus 57 pts/m^2 for LiDAR). The higher point density is able to capture more of the subtleties of the microtopography present in the grass, increasing the likelihood that the top of the vegetation is sampled at each vegetation height checkpoint.

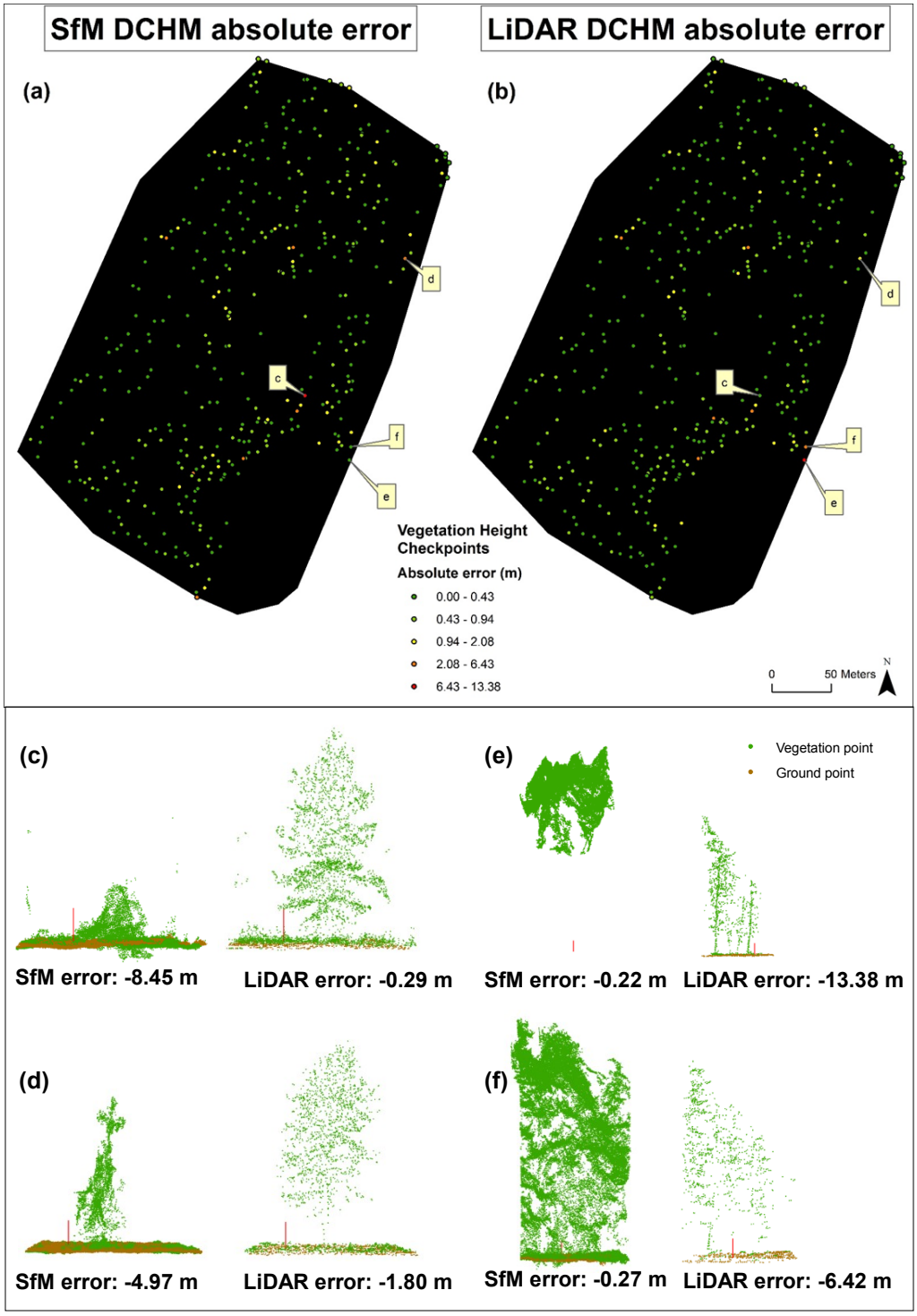

Figure 3.9 Vegetation height checkpoints and absolute errors of the (a) SfM DCHM and (b) LiDAR DCHM. Four checkpoints marked and profile views of the SfM and LiDAR point clouds below: (c) highest SfM error, (d) second highest SfM error, (e) highest LiDAR error, and (f) second highest LiDAR error. For scale, red vertical line in each profile view is 2 m.

In terms of Q_{95}, SfM was superior in measuring coniferous tree heights (i.e., SfM Q_{95} of 2.58 m and LiDAR Q_{95} of 3.31 m), but inferior in measuring deciduous tree heights (i.e., SfM Q_{95} of 2.29 m and LiDAR Q_{95} of 1.91 m). This could be explained by: (i) the simpler shape of a coniferous tree (generally conic with a distinct pointed top) and the more complex shape of a deciduous tree that may be more difficult for SfM to reconstruct, and (ii) the larger foliage of deciduous trees was more likely to reflect LiDAR pulses than the needled, thin pointed tops of the coniferous trees.

To compare the ability of SfM and LiDAR to capture ground points under trees and reconstruct coniferous and deciduous tree crowns, Figure 3.10 shows four transects and the corresponding profile views of the classified point clouds. Transect *a-a'* is positioned through deciduous trees (Balsam Poplar). The SfM point cloud contains less ground points underneath the trees. Transect *b-b'* is positioned through isolated deciduous trees (Balsam Poplar). Both point clouds contain ground points under the trees. Transect *c-c'* is positioned through coniferous trees (Lodgepole Pine). The SfM point cloud is mostly missing ground points under the trees, while the LiDAR point cloud contains ground points throughout most of the length of the transect. Transect *d-d'* is positioned through another group of coniferous trees (White Spruce) located along the edge of the coniferous tree area. Both point clouds contain ground points under the trees. In general, when SfM contains ground points under trees, they are much denser than LiDAR (i.e., average ground point spacing of 417 pts/m^2 for SfM and 11 pts/m^2 for LiDAR). However, the SfM ground point gaps account for 42% of the coniferous tree area, six times more than the LiDAR ground point gaps (i.e., 7%). The UAV-SfM data was much less consistent in capturing ground points than the UAV-LiDAR data.

These profile views also demonstrate that, although LiDAR recorded less points per tree, the points are more evenly distributed throughout the crown. SfM was not able to reconstruct portions of trees that were occluded by the canopy. The greater spatial coverage of the LiDAR canopy measurements has implications for its consistency and reliability relative to SfM for obtaining structural measurements such as crown width, depth, and volume. Tree trunks were resolved by SfM when trees were isolated, as demonstrated with the deciduous trees in transect *b-b'*, but not when canopy occluded the trunks as the other transect profile views show. Tree trunks faintly recorded by LiDAR are visible in transects a-a', b-b', and c-c'. Flying the UAV-

LiDAR system lower and/or slower would likely increase the point density and the degree of tree reconstruction. In all profiles, the SfM and LiDAR point clouds produced similar shapes for the trees, though in transect *a-a'* it appears that SfM flattened some of the deciduous tree tops. This flattening, along with the tendency for SfM to overestimate ground elevation under deciduous trees, may have contributed to LiDAR's superior performance in measuring deciduous tree heights, in addition to the aforementioned factors relating to crown geometry and foliage size.

The vegetation height 95th percentile absolute errors may be unacceptable for some applications. For instance, Q_{95} values for short grass, tall grass, short shrubs, and tall shrubs account for more than half of the maximum height of the vegetation type. The largest LiDAR vegetation height errors were expected, i.e., associated with the edges of the data collection area where even the highest scan angle did not capture the tops of trees. The largest SfM vegetation height errors were unexpected, with isolated trees in the middle of the site not being reconstructed fully despite multiple viewing angles.

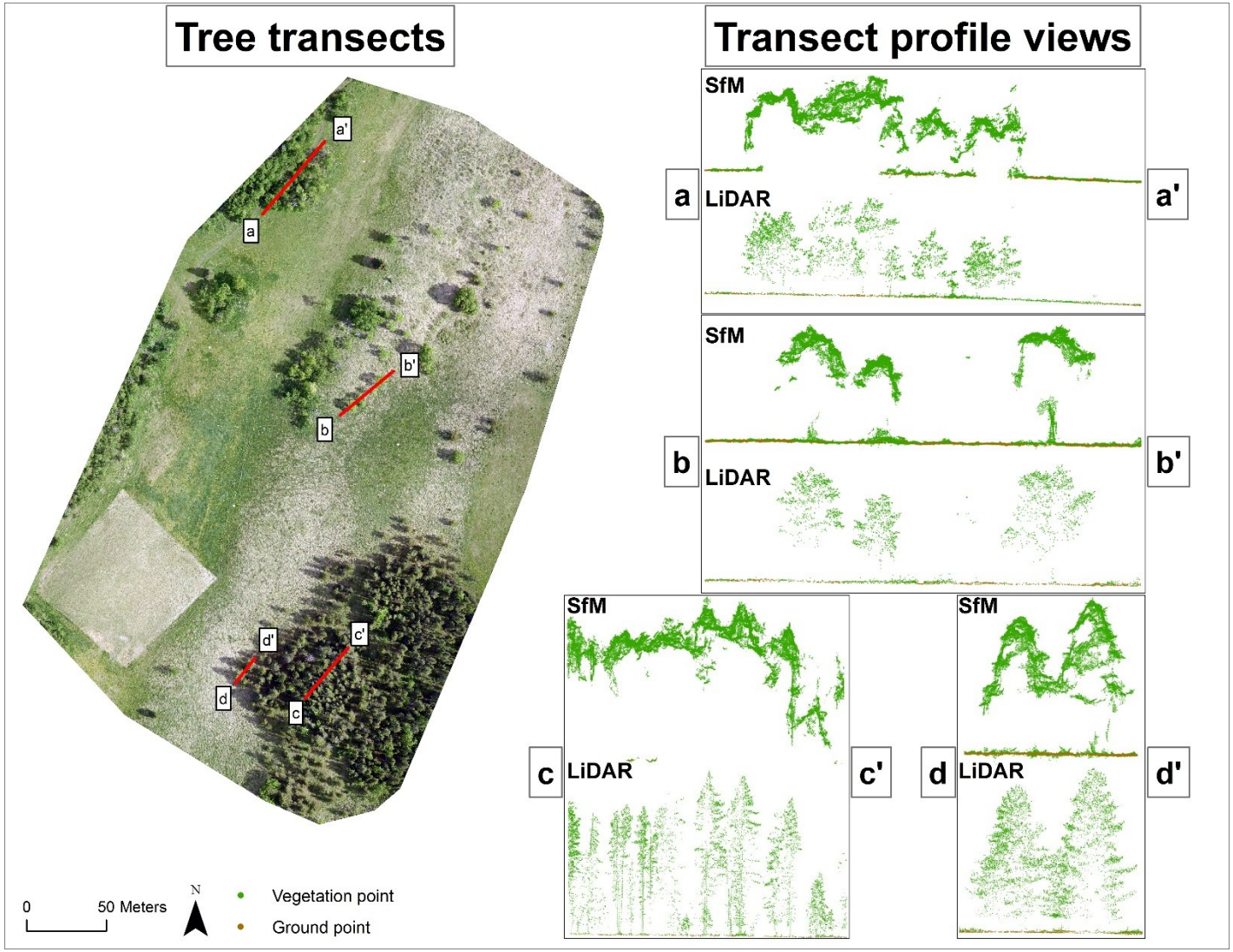

Figure 3.10 Profile view of SfM and LiDAR classified point clouds at four transects: a-a' is positioned through interior deciduous trees (Balsam Poplar), b-b' is positioned through isolated deciduous trees (Balsam Poplar), c-c' is positioned through interior coniferous trees (Lodgepole Pine), and d-d' is positioned through exterior coniferous trees (White Spruce).

3.5.4.3 Practical implications of comparison

It was demonstrated that the UAV-SfM data achieved higher vegetation height measurement accuracy in three vegetation types despite having a lower ground elevation accuracy than the UAV-LiDAR dataset. This suggests that the higher ground point density of the UAV-SfM dataset contributed to higher vegetation height accuracies due to increased likelihood of sampling the plant top. In Chapter 2, it was explained that the UAV-LiDAR flight acquired data from 60 m AGL at a speed of 15 knots. Lowering the altitude and/or the speed of the aircraft would have resulted in a higher point density, which could have potentially increased vegetation height accuracy. These flight parameters should be carefully considered along with the measurement rate of the LiDAR sensor being used in order to balance desired areal coverage with point density. The UAV-LiDAR sensor used in Chapter 2 receives up to five returns per pulse. Of the ground-classified UAV-LiDAR points, 1st, 2nd, 3rd, 4th, and 5th returns accounted for approximately 85%, 10%, 4%, 1%, and 0.1%, respectively. Considering these proportions, sensors with up to 3 returns/pulse may be suitable for vegetation mapping applications. Dual-return sensors, however, should be considered with caution. In addition to lower point density, these sensors may require a minimum distance between the two returns in order for the 2nd return to be recorded, which would prohibit dual returns in low-lying vegetation.

Our UAV-SfM imagery was captured with high overlap: 80% lateral and longitudinal, with the same configuration repeated perpendicularly. Even with this high overlap, the tops of some trees weren't fully reconstructed, and canopy occlusions prevented the sides of crowns from full reconstruction. This may limit the use of UAV-SfM from obtaining reliable measurements of crown width, depth, and volume. However, despite the incomplete reconstruction of trees and the lower ground elevation accuracy, the UAV-SfM data had a higher vegetation height accuracy in coniferous trees, short grass, and tall grass. This suggests that vegetation height may be the only structural parameter suitable for measurement with UAV-SfM. Further, UAV-SfM vegetation height measurements may be improved by increasing the obliquity of image acquisition. Following the principles of close-range photogrammetry, by increasing the image pitch angle, the angle of ray intersection between overlapping images would increase, and possibly result in more accurate canopy surface elevations (Wolf & Dewitt, 2000). Additionally, UAV-SfM vegetation height measurements may be improved with the

integration of a more accurate DTM. Specifically, the combination of a UAV-SfM DSM with a UAV-LiDAR DTM may produce a more accurate DCHM than the two methods alone.

3.6 Conclusion

We examined the accuracy of ground surface elevation and vegetation height measurements derived from a UAV-SfM dataset at a site with six vegetation types. Vertical and vegetation height accuracies were calculated as the 95th percentile absolute error (Q_{95}). The overall vertical Q_{95} value based on 862 checkpoints was 0.17 m. The UAV-SfM data meet the requirements of a 0.17 m vertical accuracy class and have a 0.51 m vegetated vertical accuracy (VVA) at the 95% confidence level (ASPRS, 2015). For vertical accuracy in vegetation types, UAV-SfM Q_{95} values ranged from 0.14 m for short grass to 0.26 m for tall shrubs. Based on statistical testing, we conclude that UAV-SfM had a tendency to overestimate ground surface elevation in all vegetation types except coniferous trees. For vegetation height accuracy based on 382 checkpoints, the overall Q_{95} value was 1.35 m. Among the vegetation types, Q_{95} values ranged from 0.22 m (short grass) to 2.58 m (coniferous trees). Based on statistical testing, we conclude that the UAV-SfM had a tendency to underestimate vegetation height in all vegetation types.

We also compared UAV-SfM ground elevation and vegetation height accuracies to the UAV-LiDAR dataset assessed in Chapter 2. The UAV-SfM data had lower ground elevation measurement accuracy overall and in every vegetation type, and had a higher tendency to overestimate ground elevation than UAV-LiDAR. UAV-SfM experienced the lowest ground elevation accuracy in tall shrubs and tall grass, whereas UAV-LiDAR experienced the lowest ground elevation accuracy in deciduous trees, short shrubs, and tall shrubs. In terms of measuring vegetation heights, UAV-SfM had lower accuracy overall and for deciduous trees, short shrubs, and tall shrubs. The lower vegetation height accuracy of UAV-SfM in these vegetation types can be explained by: (i) the complex structure of shrubs and deciduous tree crowns, which may be difficult for SfM-MVS to reconstruct, and (ii) the lower ground elevation accuracy of UAV-SfM relative to UAV-LiDAR in these vegetation types. Conversely, the higher vegetation height accuracy of UAV-SfM in coniferous trees, short grass, and tall grass, despite its lower ground elevation accuracy, could be due to the much higher average point density (i.e., 595 pts/m^2 for UAV-SfM versus 57 pts/m^2 for UAV-LiDAR). The higher point density was able

to capture the pointed tops of coniferous trees (mainly Lodgepole Pine) and the subtleties of the microtopography present in the grass, increasing the likelihood that the top of the vegetation was sampled at each vegetation height checkpoint.

The highest vegetation height errors from UAV-SfM occurred when relatively isolated trees weren't fully reconstructed, whereas the highest UAV-LiDAR vegetation height errors occurred along the edge of data collection where tree top elevations exceeded the field of view of the laser scanner. The nature of these errors – the former uncontrollable, and the latter avoidable – should prompt caution when using UAV-SfM for deriving vegetation heights. Additionally, incomplete reconstruction of the sides of tree crowns was noted upon visual inspection of the UAV-SfM point cloud. This shortcoming may limit UAV-SfM to measuring tree heights and not crown width, depth, volume, or other related structural parameters, as occlusions by canopy may be inevitable regardless of high imagery overlap, especially for complexly shaped deciduous crowns.

The ground surface elevation accuracies of UAV-SfM, ranging from 0.14-0.26 m in the vegetation types, may be acceptable for some applications in vegetated terrain. In this case, the CSF point classification algorithm was found to be computationally efficient and robust to sub-canopy ground point data gaps, and is thus recommended as a non-proprietary option for filtering UAV-SfM point clouds. If higher ground elevation accuracies are needed, then UAV-LiDAR should be used. Flying the UAV-LiDAR system at a lower altitude and/or speed would increase point density and potentially increase vegetation height accuracy. Alternatively, a UAV-LiDAR DTM can be combined with a UAV-SfM DSM to yield higher vegetation height accuracies than those obtained in this study.

Chapter 4: Conclusion

4.1 Summary of conclusions and contributions

4.1.1 Chapter 2

In Chapter 2, UAV-LiDAR data were assessed for horizontal, vertical (ground surface elevation), and vegetation height accuracies in six vegetation types (coniferous and deciduous trees, short and tall grass, and short and tall shrubs). Results determined that the data meet the requirements of a 0.02 m horizontal accuracy class and have a 0.05 m horizontal accuracy at the 95% confidence level (ASPRS, 2015). The horizontal RMSE (0.03 m) was 20 times lower than that obtained by the only other known reported UAV-LiDAR horizontal accuracy (i.e., 0.42-0.60 m) (Wallace et al., 2012; 2016). Results also showed that the data meet the requirements of a 0.08 m vertical accuracy class and have a 0.24 m vegetated vertical accuracy (VVA) at the 95% confidence level (ASPRS, 2015). Vertical error among vegetation types varied by only 0.05 m in terms of 95th percentile absolute error (Q_{95}), and ranged from 0.06 m for coniferous trees to 0.11 m for deciduous trees. However, vegetation height error varied among vegetation types by 3.03 m, ranging from 0.28 m for short grass to 3.31 m for coniferous trees. This large variation highlights the importance of considering vegetation type-specific error instead of universal, site-wide error at locations with different types of vegetation. Accordingly, this study builds on previous UAV-LiDAR accuracy assessments by: (i) applying the ASPRS (2015) methods for accuracy standards, (ii) calculating horizontal accuracy using a different technique, and obtaining a lower horizontal RMSE, (iii) calculating vertical errors of LiDAR ground surface elevation in vegetated terrain (i.e., not using artificial targets) and categorizing them by vegetation type, and (iv) calculating vegetation height errors in several vegetation types.

4.1.2 Chapter 3

In Chapter 3, UAV-SfM data were assessed for their accuracy in measuring the ground surface elevation and vegetation height at the same study site as Chapter 2. Results show that the UAV-SfM data meet the requirements of a 0.17 m vertical accuracy class and have a 0.51 m VVA at the 95% confidence level (ASPRS, 2015). Among the vegetation types, vertical error Q_{95} values ranged from 0.14 m for short grass to 0.26 m for tall shrubs. The overall vegetation height Q_{95}

was 1.35 m. Among the six vegetation types, Q_{95} values ranged from 0.22 m for short grass to 2.58 m for coniferous trees. In this chapter, we also examined the differences in ground surface elevation and vegetation height error between the UAV-SfM dataset and UAV-LiDAR dataset obtained in Chapter 2. Overall, UAV-SfM had lower accuracy in measuring ground surface elevation in every vegetation type, and lower accuracy for measuring the height of deciduous trees, short shrubs, and tall shrubs. Despite having less accurate ground surface elevation than UAV-LiDAR, the accuracy of UAV-SfM for measuring vegetation height was higher for coniferous trees, short grass, and tall grass, which could be attributed to the higher average point density of UAV-SfM (i.e., 595 pts/m^2), which increases the likelihood of capturing the top of vegetation. Lower point density in the UAV-LiDAR dataset (i.e., 57 pts/m^2) likely reduced the number of returns from the top of vegetation, thereby reducing the accuracy of height measurements derived from the UAV-LiDAR point cloud. However, for some types of vegetation, the accuracy of UAV-SfM was lower than UAV-LiDAR, which could be due to the lower accuracy of the ground surface elevation, as well as the complex structure of the vegetation types. Regarding tree reconstruction, the UAV-SfM data experienced occlusions from the canopy that prevented sampling of the sides of tree crowns, whereas the UAV-LiDAR data more consistently and evenly sampled tree crowns. This suggests that UAV-SfM data could be limited to measuring tree heights and, unless merged with data from other techniques, have limited success with other structural parameters such as crown width, depth, and volume.

This study builds on previous UAV-SfM accuracy assessments in vegetated terrain by: (i) applying the ASPRS (2015) methods for accuracy standards, (ii) assessing ground surface elevation and vegetation height errors in several different types of vegetation, and (iii) comparing those results to a UAV-LiDAR dataset acquired on the same day at the same study site.

4.2 Limitations

The UAV-SfM and UAV-LiDAR comparison in Chapter 3 was limited by methodological differences between Chapter 2 and Chapter 3, which included several notable discrepancies: (i) different point classification algorithms to filter ground points, (ii) different vertical checkpoints to calculate ground surface elevation errors, and (iii) calculating ground surface elevation errors using the interpolated values of the SfM DTM (i.e., point-to-surface method) as opposed to

values of the actual SfM points (i.e., point-to-point method). As indicated, Chapter 2 used the point-to-point method for determining accuracy of ground surface elevation, while Chapter 3 used point-to-surface. However, due to large occlusions in the UAV-SfM dataset, it was determined that the point-to-surface method was preferable so as to ensure accuracy could be evaluated in all vegetation types.

4.3 Future work

4.3.1 UAV-LiDAR and UAV-SfM accuracy comparison

Future work to improve comparability of UAV-SfM and UAV-LiDAR datasets should examine other point classification algorithms and apply a consistent classification scheme to both datasets. However, there is a possibility that the highest accuracies will not be achieved using the same method, so it will be important to examine a range of methods and algorithms. Second, the same vertical checkpoints used for UAV-LiDAR in Chapter 2 should be used in the assessment of ground surface elevation accuracy for the UAV-SfM dataset in Chapter 3. At each vertical checkpoint location, a 0.15 m radius search area (equivalent to that used for UAV-LiDAR in Chapter 2) could be used to locate a corresponding UAV-SfM point. If no UAV-SfM point is found within this search radius, the vertical checkpoint would be discarded from the analysis. By examining these approaches, the commensurability of the measurements derived from the datasets would improve and allow for more concrete conclusions to be drawn regarding the accuracy of the techniques in vegetated terrain. Further, the data could be examined using statistical testing to explore the significance of differences in errors. The tests would include median comparison tests (e.g., Mood's Median test) to examine in which vegetation types the UAV-SfM and UAV-LiDAR median errors significantly differed.

4.3.2 Improving vegetation height accuracy

Results suggest that UAV-LiDAR and UAV-SfM have complimentary properties with respect to accuracy: the former yields highly accurate ground surface elevation, while the latter performs better in recording the top of vegetation. Combining the two datasets may therefore optimize the accuracy of vegetation height. In this study, the UAV platform used for the LiDAR survey is capable of supporting both the LiDAR payload and a digital camera. Results suggest that using

both sensors during the flight, and then merging the two point clouds, may provide the best opportunity to obtain high-accuracy data.

These vegetation height measurements may be further refined by increasing the obliquity of UAV-SfM image acquisition. Following the principles of close-range photogrammetry, by increasing the image pitch angle, the angle of ray intersection between overlapping images would increase, and possibly result in more accurate canopy surface elevations (Wolf & Dewitt, 2000). Future testing should include capturing vertical and oblique imagery (at various angles) and comparing the vegetation height accuracies of the UAV-SfM datasets.

4.3.3 Regression analysis

For Chapter 2, reference measurements of ground surface elevation were obtained at UAV-LiDAR point locations. To explore possible relationships between UAV-LiDAR ground surface elevation error and different variables, multivariate regression analysis could be performed. The variables could include UAV-LiDAR point properties such as scan angle, return number, intensity, range, time, and flight strip. Variables could also include reference data parameters such as northing, easting, and elevation. For the ground elevation reference measurements obtained with the RTK GNSS, variables could include distance from the measurement to the base station, number of visible satellites, and Position Dilution of Precision.

In the same regard, reference measurements of grass and shrub heights also contain ground surface elevation measurements made by the RTK GNSS. With the ground surface elevation and vegetation height reference measurements at grass and shrub locations, DTM and DCHM error can be calculated. Linear regression of these errors should be performed to explore the relationship between the overestimation of the ground surface and underestimation of vegetation height.

4.4 Concluding remarks

As technology continues to evolve for both UAV-SfM and UAV-LiDAR, the intended impact of this research is not the accuracy results (as those will change with advances in technology), but the rigor with which the assessment was conducted. By carefully considering the recommendations of the 2015 American Society for Photogrammetry and Remote Sensing

(ASPRS) Positional Accuracy Standards for Digital Geospatial Data (ASPRS, 2015), we were able to design an accuracy assessment with the recommended quantity and spatial distribution of checkpoints and the appropriate accuracy reporting statistics. The assessment of ground elevation and vegetation height errors in different vegetation types allowed for a deeper understanding of the strengths and weaknesses of UAV-SfM and UAV-LiDAR, and – through large differences of vegetation height error occurring between vegetation types – revealed that a universal accuracy statistic (consolidating the errors of all vegetation types) may misinform practitioners about expected accuracy in vegetated terrain.

References

Andersen, H., Reutebuch, S. E., & McGaughey, R. J. (2006). A rigorous assessment of tree height measurements obtained using airborne lidar and conventional field methods. *Canadian Journal of Remote Sensing*, *32*(5), 355–366. http://doi.org/10.5589/m06-030

ASPRS. (2015). ASPRS Positional Accuracy Standards for Digital Geospatial Data. *Photogrammetric Engineering & Remote Sensing*, *81*(3), 1–26. http://doi.org/10.14358/PERS.81.3.A1-A26

Axelsson, P. (1999). Processing of laser scanner data—algorithms and applications. ISPRS Journal of Photogrammetry and Remote Sensing, 54, 138–147. http://doi.org/10.1016/S0924-2716(99)00008-8

Bater, C. W., & Coops, N. C. (2009). Evaluating error associated with lidar-derived DEM interpolation. Computers and Geosciences, 35(2), 289–300. http://doi.org/10.1016/j.cageo.2008.09.001

Carrivick, J.L., Smith, M.W., & Quincey, D.J. (2016). *Structure from Motion in the Geosciences*. West Sussex, UK: John Wiley & Sons, Ltd.

Clark, M. L., Clark, D. B., & Roberts, D. A. (2004). Small-footprint lidar estimation of sub-canopy elevation and tree height in a tropical rain forest landscape. *Remote Sensing of Environment*, *91*(1), 68–89. http://doi.org/10.1016/j.rse.2004.02.008

Csanyi, N., & Toth, C. K. (2007). Improvement of Lidar Data Accuracy Using Lidar-Specific Ground Targets. *Photogrammetric Engineering & Remote Sensing*, *73*(4), 385–396.

Dandois, J. P., & Ellis, E. C. (2010). Remote sensing of vegetation structure using computer vision. *Remote Sensing*, *2*(4), 1157–1176. http://doi.org/10.3390/rs2041157

Dandois, J. P., & Ellis, E. C. (2013). High spatial resolution three-dimensional mapping of vegetation spectral dynamics using computer vision. *Remote Sensing of Environment*, *136*, 259–276. http://doi.org/10.1016/j.rse.2013.04.005

Erdody, T. L., & Moskal, L. M. (2010). Fusion of LiDAR and imagery for estimating forest canopy fuels. Remote Sensing of Environment, 114(4), 725–737. http://doi.org/10.1016/j.rse.2009.11.002

Evans, J. S., & Hudak, A. T. (2007). A multiscale curvature algorithm for classifying discrete return LiDAR in forested environments. *IEEE Transactions on Geoscience and Remote Sensing*, *45*(4), 1029–1038. http://doi.org/10.1109/TGRS.2006.890412

Gatziolis, D., Fried, J. S., & Monleon, V. S. (2010). Challenges to estimating tree height via LiDAR in closed-canopy forests: A parable from Western Oregon. Forest Science, 56(2), 139–155.

Gaveau, D., & Hill, R. (2003). Quantifying canopy height underestimation by laser pulse penetration in small-footprint airborne laser scanning data. *Canadian Journal of Remote Sensing*, *29*(5), 650–657.

Glenn, N. F., Spaete, L. P., Sankey, T. T., Derryberry, D. R., Hardegree, S. P., & Mitchell, J. (2011). Errors in LiDAR-derived shrub height and crown area on sloped terrain. *Journal of Arid Environments*, *75*(4), 377–382. http://doi.org/10.1016/j.jaridenv.2010.11.005

Hirata, Y. (2004). The effects of footprint size and sampling density in airborne laser scanning to extract individual trees in mountainous terrain. *International Archives for Photogrammetry, Remote Sensing and Spatial Information Sciences*, *36*(8), 102–107. Retrieved from http://www.isprs.org/proceedings/XXXVI/8-W2/HIRATA.pdf

Hodgson, M. E., & Bresnahan, P. (2004). Accuracy of Airborne Lidar-Derived Elevation : Empirical Assessment and Error Budget. *Photogrammetric Engineering & Remote Sensing*, *70*(3), 331–339.

Hodgson, M. E., Jensen, J., Raber, G., Tullis, J., Davis, B. a, Thompson, G., & Schuckman, K. (2005). An Evaluation of Lidar-derived Elevation and Terrain Slope in Leaf-off Conditions. *Photogrammetric Engineering & Remote Sensing*, *71*(7), 817–823. http://doi.org/10.14358/PERS.71.7.817

Hopkinson, C., Chasmer, L. E., Sass, G., Creed, I. F., Sitar, M., Kalbfleisch, W., & Treitz, P. (2005). Vegetation class dependent errors in lidar ground elevation and canopy height estimates in a boreal wetland environment. *Canadian Journal of Remote Sensing*, *31*(2), 191–206. http://doi.org/10.5589/m05-007

Hugenholtz, C. H., Whitehead, K., Brown, O. W., Barchyn, T. E., Moorman, B. J., LeClair, A., … Hamilton, T. (2013). Geomorphological mapping with a small unmanned aircraft system

(sUAS): Feature detection and accuracy assessment of a photogrammetrically-derived digital terrain model. *Geomorphology*, *194*, 16–24. http://doi.org/10.1016/j.geomorph.2013.03.023

Hugenholtz, C. H., Walker, J., Brown, O., & Myshak, S. (2015). Earthwork Volumetrics with an Unmanned Aerial Vehicle and Softcopy Photogrammetry. *Journal of Surveying Engineering*, *141*(1), 6014003. http://doi.org/10.1061/(ASCE)SU.1943-5428.0000138

Hugenholtz, C.H., Brown, O., Walker, J., Barchyn, T.E., Nesbit, P.R., Kucharczyk, M., & Myshak, S. (2016). Spatial accuracy of UAV-derived orthoimagery and topography: comparing photogrammetric models processed with direct georeferencing and ground control points. *Geomatica, 70*(1), 21-30.

Jensen, J., & Mathews, A. (2016). Assessment of Image-Based Point Cloud Products to Generate a Bare Earth Surface and Estimate Canopy Heights in a Woodland Ecosystem. *Remote Sensing*, *8*(1), 50. http://doi.org/10.3390/rs8010050

Johnson, K., Nissen, E., Saripalli, S., Arrowsmith, J. R., McGarey, P., Scharer, K., … Blisniuk, K. (2014). Rapid mapping of ultrafine fault zone topography with structure from motion. *Geosphere*, *10*(5), 969–986. http://doi.org/10.1130/GES01017.1

Kwak, D.-A., Lee, W.-K., Lee, J.-H., Biging, G. S., & Gong, P. (2007). Detection of individual trees and estimation of tree height using LiDAR data. *Journal of Forest Research*, *12*(6), 425–434. http://doi.org/10.1007/s10310-007-0041-9

Lin, Y., Hyyppa, J., & Jaakkola, A. (2011). Mini-UAV-Borne LIDAR for Fine-Scale Mapping. *IEEE Geoscience and Remote Sensing Letters*, *8*(3), 426–430. http://doi.org/10.1109/LGRS.2010.2079913

Lisein, J., Pierrot-Deseilligny, M., Bonnet, S., & Lejeune, P. (2013). A photogrammetric workflow for the creation of a forest canopy height model from small unmanned aerial system imagery. *Forests*, *4*(4), 922–944. http://doi.org/10.3390/f4040922

Madden, M., Jordan, T., Bernardes, S., Cotton, D.L., O'Hare, N., & Pasqua, A. (2015). Unmanned Aerial Systems and Structure from Motion Revolutionize Wetlands Mapping. In R.W. Tiner, M.W. Lang, & V.V. Klemas (Eds.), *Remote Sensing of Wetlands: Applications and Advances* (pp. 195–220). Boca Raton, FL: CRC Press.

Maltamo, M., Mustonen, K., Hyyppä, J., Pitkänen, J., & Yu, X. (2004). The accuracy of estimating individual tree variables with airborne laser scanning in a boreal nature reserve. *Canadian Journal of Forest Research*, *34*(9), 1791–1801. http://doi.org/10.1139/x04-055

Niethammer, U., James, M. R., Rothmund, S., Travelletti, J., & Joswig, M. (2012). UAV-based remote sensing of the Super-Sauze landslide: Evaluation and results. *Engineering Geology*, *128*, 2–11. http://doi.org/10.1016/j.enggeo.2011.03.012

Persson, Å., Holmgren, J., & Söderman, U. (2002). Detecting and measuring individual trees using an airborne laser scanner. *Photogrammetric Engineering & Remote Sensing*, *68*(9), 925–932. http://doi.org/0099-lll2/02/6809-925$3.0

Slattery, K. T., & Slattery, D. K. (2013). Modeling Earth Surfaces for Highway Earthwork Computation Using Terrestrial Laser Scanning. *International Journal of Construction Education and Research*, *9*(March), 132–146. http://doi.org/10.1080/15578771.2012.700298

St-Onge, B., Hu, Y., & Véga, C. (2008). Mapping the height and above-ground biomass of a mixed forest using lidar and stereo Ikonos images. International Journal of Remote Sensing, 29(5), 1277–1294. http://doi.org/10.1080/01431160701736505

Streutker, D. R., & Glenn, N. F. (2006). LiDAR measurement of sagebrush steppe vegetation heights. *Remote Sensing of Environment*, *102*(1–2), 135–145. http://doi.org/10.1016/j.rse.2006.02.011

Suarez, J. C., Ontiveros, C., Smith, S., & Snape, S. (2005). Use of airborne LiDAR and aerial photography in the estimation of individual tree heights in forestry. *Computers and Geosciences*, *31*(2), 253–262. http://doi.org/10.1016/j.cageo.2004.09.015

Tamminga, A. D., Eaton, B. C., & Hugenholtz, C. H. (2015). UAS-based remote sensing of fluvial change following an extreme flood event. *Earth Surface Processes and Landforms*, *40*(11), 1464–1476. http://doi.org/10.1002/esp.3728

Tang, L., & Shao, G. (2015). Drone remote sensing for forestry research and practices. *Journal of Forestry Research*, *26*(4), 791–797. http://doi.org/10.1007/s11676-015-0088-y

Tinkham, W. T., Huang, H., Smith, A. M. S., Shrestha, R., Falkowski, M. J., Hudak, A. T., … Marks, D. G. (2011). A Comparison of two open source LiDAR surface classification algorithms. *Remote Sensing*, *3*(3), 638–649. http://doi.org/10.3390/rs3030638

Vastaranta, M., Wulder, M. A., White, J. C., Pekkarinen, A., Tuominen, S., Ginzler, C., … Hyyppä, H. (2013). Airborne laser scanning and digital stereo imagery measures of forest structure: Comparative results and implications to forest mapping and inventory update. Canadian Journal of Remote Sensing, 39(5), 382–395. http://doi.org/10.5589/m13-046

Véga, C., & St-Onge, B. (2008). Height growth reconstruction of a boreal forest canopy over a period of 58 years using a combination of photogrammetric and lidar models. Remote Sensing of Environment, 112(4), 1784–1794. http://doi.org/10.1016/j.rse.2007.09.002

Wallace, L., Lucieer, A., Turner, D., & Watson, C. (2011). Error assessment and mitigation for hyper-temporal UAV-borne LiDAR surveys of forest inventory. *SilviLaser*, (2010), 1–9.

Wallace, L., Lucieer, A., Watson, C., & Turner, D. (2012). Development of a UAV-LiDAR System with Application to Forest Inventory. *Remote Sensing*, *4*(12), 1519–1543. http://doi.org/10.3390/rs4061519

Wallace, L., Musk, R., & Lucieer, A. (2014). An assessment of the repeatability of automatic forest inventory metrics derived from UAV-borne laser scanning data. *IEEE Transactions on Geoscience and Remote Sensing*, *52*(11), 7160–7169. http://doi.org/10.1109/TGRS.2014.2308208

Wallace, L., Lucieer, A., Malenovský, Z., Turner, D., & Vopěnka, P. (2016). Assessment of Forest Structure Using Two UAV Techniques: A Comparison of Airborne Laser Scanning and Structure from Motion (SfM) Point Clouds. *Forests*, *7*(3), 62. http://doi.org/10.3390/f7030062

Westoby, M. J., Brasington, J., Glasser, N. F., Hambrey, M. J., & Reynolds, J. M. (2012). "Structure-from-Motion" photogrammetry: A low-cost, effective tool for geoscience applications. *Geomorphology*, *179*, 300–314. http://doi.org/10.1016/j.geomorph.2012.08.021

Whitehead, K., Moorman, B. J., & Hugenholtz, C. H. (2013). Brief Communication: Low-cost, on-demand aerial photogrammetry for glaciological measurement. *Cryosphere*, *7*(6), 1879–1884. http://doi.org/10.5194/tc-7-1879-2013

Whitehead, K., & Hugenholtz, C. H. (2014). Remote sensing of the environment with small unmanned aircraft systems (UASs), part 1: a review of progress and challenges. Journal of Unmanned Vehicle Systems, 2(3), 86–102. http://doi.org/10.1139/juvs-2014-0007

Wolf, P.R., & Dewitt, B.A. (2000). *Elements of Photogrammetry with Applications in GIS* (3rd ed.). New York, New York: McGraw-Hill.

Zarco-Tejada, P. J., Diaz-Varela, R., Angileri, V., & Loudjani, P. (2014). Tree height quantification using very high resolution imagery acquired from an unmanned aerial vehicle (UAV) and automatic 3D photo-reconstruction methods. European Journal of Agronomy, 55, 89–99.

Zhang, W., Qi, J., Wan, P., Wang, H., Xie, D., Wang, X., & Yan, G. (2016). An easy-to-use airborne LiDAR data filtering method based on cloth simulation. *Remote Sensing*, *8*(6), 1–22. http://doi.org/10.3390/rs8060501

Zimble, D. A., Evans, D. L., Carlson, G. C., Parker, R. C., Grado, S. C., & Gerard, P. D. (2003). Characterizing vertical forest structure using small-footprint airborne LiDAR. *Remote Sensing of Environment*, *87*(2–3), 171–182. http://doi.org/10.1016/S0034-4257(03)00139-1